

Quantum SU(1,1) interferometers: Basic principles and applications ^F

Cite as: APL Photonics 5, 080902 (2020); <https://doi.org/10.1063/5.0004873>

Submitted: 19 February 2020 • Accepted: 17 July 2020 • Published Online: 10 August 2020

 Z. Y. Ou and  Xiaoying Li

COLLECTIONS

 This paper was selected as Featured



View Online



Export Citation



CrossMark

ARTICLES YOU MAY BE INTERESTED IN

[Photonic quantum metrology](#)

AVS Quantum Science **2**, 024703 (2020); <https://doi.org/10.1116/5.0007577>

[Photonic quantum information processing: A concise review](#)

Applied Physics Reviews **6**, 041303 (2019); <https://doi.org/10.1063/1.5115814>

[Quantum dense metrology by an SU\(2\)-in-SU\(1,1\) nested interferometer](#)

Applied Physics Letters **117**, 024003 (2020); <https://doi.org/10.1063/5.0012304>



THE ADVANCED MATERIALS MANUFACTURER®

semiconductors	nanoparticles	perovskites	MOQVD	beta boron boron	rare earth metals	quantum dots	carbon	scintillation Ce:YAG	refractory metals	laser crystals	oxide	lithium niobate	bulk wafers	aluminum nitride	MOFs	chalcogenides	AgS	SiGe	perovskite crystals	transparent ceramics
epitaxial crystal growth	ultra high purity materials	transparent ceramics	CMOS	comet	nanoscale	nanoscale	nanoscale	nanoscale	nanoscale	nanoscale	nanoscale	nanoscale	nanoscale	nanoscale	nanoscale	nanoscale	nanoscale	nanoscale	nanoscale	nanoscale

The Next Generation of Material Science Catalogs



Quantum SU(1,1) interferometers: Basic principles and applications

Cite as: APL Photon. 5, 080902 (2020); doi: 10.1063/5.0004873

Submitted: 19 February 2020 • Accepted: 17 July 2020 •

Published Online: 10 August 2020



Z. Y. Ou^{1,2,a)}  and Xiaoying Li^{1,a)} 

AFFILIATIONS

¹College of Precision Instrument and Opto-Electronics Engineering, Key Laboratory of Opto-Electronics Information Technology, Ministry of Education, Tianjin University, Tianjin 300072, People's Republic of China

²Department of Physics, Indiana University-Purdue University Indianapolis, Indianapolis, Indiana 46202, USA

^{a)}Authors to whom correspondence should be addressed: xiaoyingli@tju.edu.cn and zou@iupui.edu

ABSTRACT

A new type of quantum interferometer was recently realized that employs parametric amplifiers (PAs) as the wave splitting and mixing elements. The quantum behavior stems from the PAs, which produce quantum entangled fields for probing the phase change signal in the interferometer. This type of quantum entangled interferometer exhibits some unique properties that are different from traditional beam splitter-based interferometers such as Mach-Zehnder interferometers. Because of these properties, it is superior to the traditional interferometers in many aspects, especially in the phase measurement sensitivity. We will review its unique properties and applications in quantum metrology and sensing, quantum information, and quantum state engineering.

© 2020 Author(s). All article content, except where otherwise noted, is licensed under a Creative Commons Attribution (CC BY) license (<http://creativecommons.org/licenses/by/4.0/>). <https://doi.org/10.1063/5.0004873>

I. INTRODUCTION

Interferometry, a technique based on wave interference, played a crucial part in the development of fundamental ideas in physics as well as in the technological advances of mankind. It has become an indispensable part in precision measurement and metrology ever since its inception. Most of the physical quantities such as distance, local gravity fields, and magnetic fields that can be measured by the interferometric technique are associated with the phases of the interfering waves. It is the extreme sensitiveness to the phase change in interferometry that leads to wide applications of the technique in precision measurement and metrology.

In traditional interferometry, as shown in Fig. 1(a), an input field is split into two by a beam splitter (BS1). One of the beams, serving as the probe, is phase modulated so as to encode a phase change (δ) onto it. It then interferes with the other beam, serving as a reference, at another beam splitter (BS2). This converts the phase change to an intensity change, and the outputs of BS2 are directly measured and analyzed with intensity detectors. Regardless of the difference in design between different schemes, the sensitivity of traditional interferometers is limited by the vacuum

quantum noise or the so-called shot noise inherited from the input field and the vacuum field injected from the unused BS input ports¹ [dashed line in Fig. 1(a)]. The sensitivity limit of this kind of interferometer is referred to as the shot noise limit (SNL) or sometimes the standard quantum limit (SQL), i.e., the general $1/\sqrt{N}$ -dependence at a large phase sensing photon number N . In order to reduce the vacuum quantum noise, squeezed states are properly injected into interferometers by replacing the vacuum state.¹ The result of the squeezed state injection is the reduction of the detection noise below the shot noise level and thus the enhancement of phase measurement sensitivity. Experimental efforts and progress were made in the generation and application of these quantum states to optical interferometry systems.^{2,3} In fact, such a technique was recently applied to km-scale large size interferometers with the goal of improving the sensitivity for gravitational wave detection.⁴⁻⁶

SU(1,1) interferometers are a new type of quantum interferometers, which are quite different from the traditional interferometers in that the linear beam splitters are replaced by nonlinear optical devices of parametric amplifiers (PAs), as shown in Fig. 1(b). The name of SU(1,1) stems from the type of interaction involved in

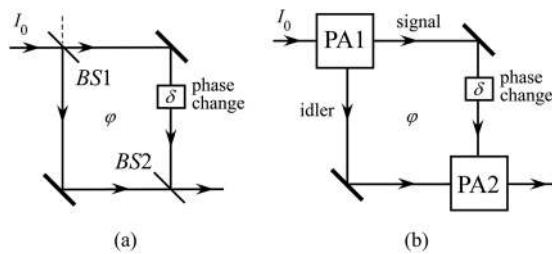


FIG. 1. Comparison between (a) a traditional Mach-Zehnder interferometer and (b) an SU(1,1) interferometer.

parametric processes for nonlinear wave mixing, which is different from the SU(2)-type interaction for linear wave mixing by a beam splitter. SU(1,1) interferometers were first proposed by Yurke *et al.*⁷ to reach the Heisenberg limit (HL), i.e., the general $1/N$ -dependence at a large phase sensing photon number N . This is the ultimate quantum limit⁸ in precision phase measurement at large N although it can be broken⁹ at small N . However, the original version is not practical because it starts with vacuum and thus has a low photon number. That is why there was no experimental implementation until recently when a modified version with a photon number boost by coherent state injection was proposed,^{10,11} which has since been realized in atomic four-wave mixing,^{12–15} bulk $\chi^{(2)}$ -nonlinear medium,¹⁶ and nonlinear optical fiber.^{17–19} In the meanwhile, theoretical investigations on SU(1,1) interferometers were also carried out for various input states and different measurement strategies^{20–22} and were based on quantum Fisher information, leading to the quantum Cramér–Rao bound.^{21,23–26}

The difference between SU(1,1) interferometers and traditional interferometers lies in the beam splitting and mixing elements. Parametric amplifiers are active quantum devices that generate quantum fields, whereas beam splitters are passive devices and rely on injection of quantum states to achieve quantum advantages. So, compared to the traditional interferometers with quantum state injections, SU(1,1) interferometers exhibit some distinct features that make them more desirable in practical applications. The first one is that the involvement of nonlinear optical processes for wave mixing allows the coherent superpositions of waves of different types such as atomic spin waves, light waves, and acoustic waves. This type of mixing is impossible for linear beam splitters. The second is that the employment of parametric amplifiers leads to amplified noise levels at outputs that are much larger than the vacuum noise level. This means the outputs are immune to losses, which are detrimental to quantum information because of the vacuum noise coupled in through the loss channels. The third is that the quantum entanglement generated by parametric amplifiers leads to correlated quantum noise, which can be canceled at destructive interference. This gives rise to higher signal amplification than noise amplification and thus improved the signal-to-noise ratio (SNR) or enhanced sensitivity.

Interference effects involving nonlinear optical processes were demonstrated as soon as the nonlinear optical effects such as second harmonic generation were discovered.²⁷ Because of the involvement of nonlinear optical processes, these nonlinear interference

effects have some interesting applications in spectroscopy,²⁸ optical imaging,^{29,30} and spatial and temporal shaping.^{31,32} They can be mostly understood with classical wave theory. At the quantum level of single photons when the gain of the parametric amplifiers is low, interferometers consisting of spontaneous parametric down-conversion were used to study two-photon or multi-photon interference,^{33,34} which cannot be explained by classical theory. These quantum interferometric effects are the basis for optical quantum information sciences.³⁵ Moreover, recently a mind-boggling photon interference effect³⁶ between two spontaneous parametric processes also found interesting applications in quantum imaging with undetected photons.^{37–41} All these phenomena were recently reviewed in a comprehensive article.⁴²

On the other hand, when the gain of the parametric amplifiers in SU(1,1) interferometers is high, the quantum noise performance of the interferometers is totally different. Early research development of SU(1,1) interferometers in this regime was covered in the comprehensive review article.⁴² However, since the publication of the article, there has been significant progress in the field, especially in the realization of many variations of the SU(1,1) interferometer and its applications in quantum metrology, quantum information, and quantum state engineering that are not covered by the review article. Furthermore, there is some misunderstanding in the early research about the working principle of the interferometer for sensitivity improvement, which leads to non-optimized performance. The roles of each nonlinear element in the interferometer were also better understood now, which reveals the underlying physics of the interferometer.

In this paper, we will explain the basic working principle of SU(1,1) interferometers with the goal of practical implementation and applications. We will concentrate on the quantum noise performance of SU(1,1) interferometers in the high gain regime with an emphasis on improving the phase measurement sensitivity. We will have an in-depth discussion on the special features of the interferometer in this case, especially on the role played by quantum entanglement. Based on this discussion, we will find the optimum operation conditions for the best performance in the form of phase measurement sensitivity and compare it to the optimum classical measurement sensitivity. We will reveal the difference and similarity between SU(1,1) interferometers and squeezed state-based traditional interferometers. These are covered in Secs. II and III. For the experimental implementation of SU(1,1) interferometers, we will review in Secs. IV and V recent realizations of different forms of the interferometer including those with different types of waves. We will discuss in Sec. VI its applications in multi-parameter measurement, quantum information splitting, quantum entanglement measurement, and mode engineering of quantum states. We conclude in Sec. VII with prospects for future development.

II. PERFORMANCE OF TRADITIONAL INTERFEROMETRY

The interferometry technique is usually based on interferometers such as the Mach-Zehnder (MZ) type shown in Fig. 2, where an incoming field in a coherent state of $|\alpha\rangle$ is split by a beam splitter (BS1) of transmissivity T_1 and reflectivity R_1 and then recombined by another of the same type (BS2) but of transmissivity T_2 and

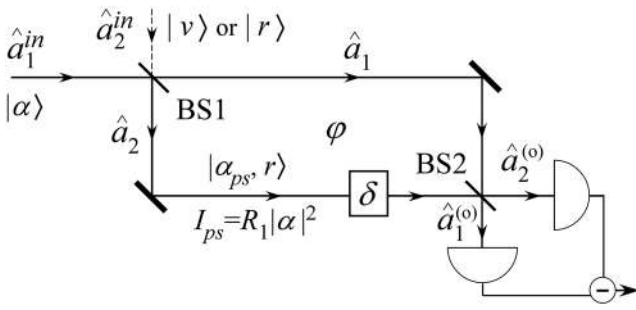


FIG. 2. A traditional Mach-Zehnder interferometer with vacuum ($|v\rangle$) or squeezed ($|r\rangle$) states at the unused port (dashed line). $|\alpha_{ps}, r\rangle$ is a coherent squeezed state with $\alpha_{ps} = \alpha\sqrt{R_1}$ for phase sensing.

reflectivity R_2 . It is straightforward to find the photon number outputs of the interferometer given by

$$\begin{aligned} I_1^{(o)} &= |\alpha|^2 (T_1 T_2 + R_1 R_2 - 2\sqrt{T_1 T_2 R_1 R_2} \cos \varphi), \\ I_2^{(o)} &= |\alpha|^2 (T_1 R_2 + R_1 T_2 + 2\sqrt{T_1 T_2 R_1 R_2} \cos \varphi), \end{aligned} \quad (1)$$

where φ is the overall phase difference between the two arms of the interferometer and $T_{1,2} + R_{1,2} = 1$. Note the energy conservation: $I_1^{(o)} + I_2^{(o)} = |\alpha|^2 \equiv I_{in}$. For a small phase change δ , which is to be measured, the change in the output photon number is

$$\delta I_1^{(o)} = -\delta I_2^{(o)} = 2|\alpha|^2 \delta \sqrt{T_1 T_2 R_1 R_2} \sin \varphi. \quad (2)$$

Because the two outputs are 180° out of phase, we can make full use of the two outputs by measuring the difference $I_-^{(o)} = I_1^{(o)} - I_2^{(o)}$, which gives twice the change,

$$\delta I_-^{(o)} = 4|\alpha|^2 \delta \sqrt{T_1 T_2 R_1 R_2} \sin \varphi. \quad (3)$$

Obviously, the change $\delta I_-^{(o)}$ is maximum when $\varphi = \pi/2$, which is the operational point we will take in the following.

The measurement sensitivity, on the other hand, depends on the noise level at detection. For the input of a coherent state $|\alpha\rangle$, the detection noise is the photon number fluctuation, which has the Poissonian statistics: $\langle \Delta^2 I_{1,2}^{(o)} \rangle = I_{1,2}^{(o)}$. Since the two outputs are also in coherent states so that their fluctuations are uncorrelated quantum mechanically, we have

$$\langle \Delta^2 I_-^{(o)} \rangle = \langle \Delta^2 I_1^{(o)} \rangle + \langle \Delta^2 I_2^{(o)} \rangle = I_1^{(o)} + I_2^{(o)} = |\alpha|^2. \quad (4)$$

If the signal-to-noise ratio (SNR) is defined as

$$\text{SNR} \equiv \frac{(\delta I_-^{(o)})^2}{\langle \Delta^2 I_-^{(o)} \rangle}, \quad (5)$$

we obtain the SNR for the MZ interferometer,

$$\text{SNR}_{MZ} = 16|\alpha|^2 \delta^2 T_1 T_2 R_1 R_2 = 16T_1 T_2 R_2 I_{ps} \delta^2, \quad (6)$$

where $I_{ps} \equiv R_1 |\alpha|^2 = I_2$ is the number of photons in the field that probes the phase change. This quantity is an important figure of merit for fair comparison of different schemes of phase measurement. With $T_2 + R_2 = 1$, we find the optimum SNR,

$$\text{SNR}_{MZ}^{(op)} = 4I_{ps} \delta^2, \quad (7)$$

when $T_2 = R_2 = 1/2$ and $T_1 \rightarrow 1$. The minimum measurable phase shift is $\delta_m = 1/2\sqrt{I_{ps}}$ when $\text{SNR}_{MZ}^{(op)} = 1$. This is the optimum phase measurement sensitivity that is achievable with a classical probing field for a given phase sensing photon number I_{ps} . Since the detection noise is from photon number fluctuation of Poissonian nature and is the same as the shot noise in an electric current, this phase measurement sensitivity is known as “the shot noise limit (SNL),” a term preferred by experimentalists. Moreover, since the photon number fluctuation is originated from quantum nature of light, this limit is also called “standard quantum limit (SQL)” of phase measurement, a term favored by theorists.

Note that the optimum condition $T_1 \approx 1$ leads to extremely unbalanced photon numbers in the two arms of the interferometer. This is in contrast to the popular balanced implementation of the interferometer.^{2,11} This gives rise to the controversy of two classical limits of phase measurement for the comparison with quantum measurement.⁴³ However, the unbalanced scheme is consistent with the homodyne measurement technique where the local oscillator (LO) has much stronger intensity than the signal field. Here, in the unbalanced scheme, the phase-encoded field (\hat{a}_2) can be regarded as the signal field to be measured, whereas the other arm (\hat{a}_1) with a much larger photon number is treated as the LO. The condition of $T_2 = R_2 = 1/2$ corresponds to balanced homodyne measurement.⁴⁴ Thus, the balanced homodyne measurement technique achieves the optimum phase measurement sensitivity in classical interferometry.

Perhaps, a better way to understand why we need to have an unbalanced interferometer for optimum sensitivity is through the intrinsic phase uncertainty $\Delta^2 \varphi$ in any optical field.⁴⁵ The interference method measures the phase difference $\varphi = \varphi_1 - \varphi_2$ so that the measurement uncertainty is $\Delta^2 \varphi = \Delta^2 \varphi_1 + \Delta^2 \varphi_2$ if the phase fluctuations in the two arms are independent (indeed, the quantum fluctuations are independent for coherent states). However, it was shown⁴⁵ that the intrinsic phase uncertainty $\Delta^2 \varphi_i (i = 1, 2)$ is inversely proportional to I_i . Making $I_1 \gg I_2$ gives $\Delta^2 \varphi_1 \ll \Delta^2 \varphi_2$ so that $\Delta^2 \varphi \approx \Delta^2 \varphi_2 = \Delta^2 \varphi_{ps} \sim 1/I_{ps}$ (the subscript ps denotes the phase sensing field). However, for a balanced interferometer, $I_1 = I_2$ or $\Delta^2 \varphi_1 = \Delta^2 \varphi_2$, so we have $\Delta^2 \varphi = 2\Delta^2 \varphi_{ps}$. Hence, the unbalanced interferometer has half the measurement uncertainty as the balanced one¹¹ and thus better sensitivity with twice the SNR.⁴³

Note that, here, we only use one arm for sensing and the optimum condition is $T_1 \approx 1 \gg R_1$. If two arms are used for sensing such as the situations of Sagnac interferometers for rotation sensing and Laser Interferometer Gravitational Wave Observatory (LIGO) for gravitational wave sensing, the optimum condition will be $T_1 = R_1 = 1/2$ to give balanced interferometers.

The shot noise limit can be surpassed if we inject a squeezed state $|r\rangle$ into the unused port \hat{a}_2^{in} (dashed line) of the interferometer,¹ as shown in Fig. 2. Under the optimum operational condition of $T_2 = R_2 = 1/2$ and $T_1 \rightarrow 1$, $R_1 \ll 1$, the probe field becomes a coherent squeezed state $|\alpha_{ps}, r\rangle$ with $\alpha_{ps} = \alpha\sqrt{R_1}$ and squeezing parameter r , which is related to the amplitude gains $G = \cosh r$, $g = \sinh r$ ($r > 0$) of a degenerate parametric amplifier generating the squeezed state.⁴⁶ As mentioned before, the second BS is equivalent to a balanced homodyne measurement and it is straightforward to find the

photon number fluctuation at this time as⁴⁴

$$\langle \Delta^2 I_-^{sq} \rangle = |\alpha|^2 e^{-2r} = |\alpha|^2 / (G + g)^2, \quad (8)$$

which gives rise to the signal-to-noise ratio as

$$SNR_{MZ}^{sq} = 4I_{ps}\delta^2 (G + g)^2. \quad (9)$$

Note that this SNR for the squeezed state interferometry has an enhancement factor of $(G + g)^2 = e^{2r}$ compared to the optimum classical SNR in Eq. (7) or $\delta_m^{sq} = e^{-r}/2\sqrt{I_{ps}} = \delta_m e^{-r}$ when $SNR_{MZ}^{sq} = 1$. Since the detection noise in Eq. (8) is smaller than the shot noise level in Eq. (4), this leads to the sub-shot noise interferometry.^{2,3}

In the expressions above, we assumed $R_1|\alpha|^2 \gg g^2 = \sinh^2 r$ so that the coherent state provides most of the photons for phase sensing. At a large r -value, the squeezed state contributes a sizable photon number for I_{ps} and optimization between r and α will lead to the so-called Heisenberg limit of phase measurement.^{47,48}

In practice, interferometers are usually operated at the dark fringe mode. This is because high sensitivity requires high I_{ps} [see Eq. (7)], which can saturate the detectors. This requires $\varphi = \pi$, $T_1 = T_2 \gg R_1 = R_2$. To avoid electronic noise, homodyne measurement is performed at the dark port ($\hat{a}_2^{(o)}$). In this case, the output noise is simply the vacuum noise or the squeezed noise from the unused input port ($\hat{a}_2^{(in)}$ in Fig. 2), so it can be easily shown¹ that the SNR in this case is the same as the optimized classical SNR given by Eq. (7) or the squeezed state case given by Eq. (9).

III. SU(1,1) INTERFEROMETERS

A new type of interferometer, known as the so-called “SU(1,1) interferometer,”^{7,10–13} is formed when we replace the beam splitters in a Mach-Zehnder interferometer (MZI) with parametric amplifiers (Fig. 3), which can split and mix two input fields coherently for interference. It is well known that parametric amplifiers are active devices and produce quantum states by themselves,^{49,50} so the fields inside the interferometers possess some unique quantum behaviors even without the input of quantum fields. This new type of interferometer is of quantum nature by itself and will exhibit some advantages over traditional interferometers.

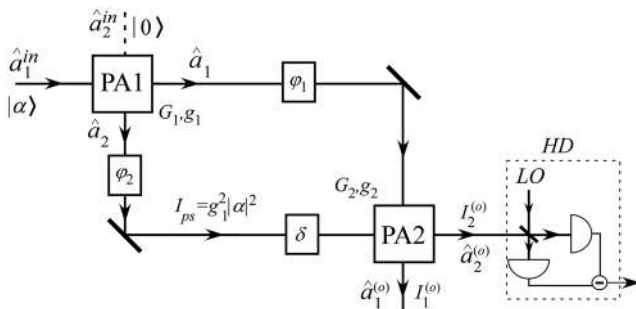


FIG. 3. SU(1,1) interferometer, where beam splitters of traditional interferometers are replaced by parametric amplifiers (PA1, PA2) of gain G_1 , G_2 , respectively. $I_{ps} = g_1^2|\alpha|^2$ is the photon number of the field sensing the phase change δ .

A. Parametric amplifiers as beam splitters

Parametric amplifiers are a result of three-wave or four-wave mixing in a nonlinear optical process. The interaction Hamiltonian is in the form of

$$\hat{H}_{PA} = i\hbar\xi\hat{a}_1^\dagger\hat{a}_2^\dagger - i\hbar\xi^*\hat{a}_1\hat{a}_2, \quad (10)$$

where ξ is some parameter proportional to the nonlinear coefficient and the amplitudes of strong pump fields, which can be treated as classical waves. The other two relatively weak fields are the quantum fields described by the operators \hat{a}_1 , \hat{a}_2 . To have better comparison with traditional interferometers with BS, we use the Heisenberg picture here and describe the system with operator evolution. The input and the output relation of the quantum fields for the Hamiltonian in Eq. (10) are

$$\hat{a}_1^{(o)} = G\hat{a}_1^{(in)} + g\hat{a}_2^{(in)\dagger}, \quad \hat{a}_2^{(o)} = G\hat{a}_2^{(in)} + g\hat{a}_1^{(in)\dagger}, \quad (11)$$

with $G = \cosh r$, $g = \sinh r$ as the amplitude gains and $r \propto \xi$. Note that we set the phase of r to zero for convenience without loss of generality.

If quadrature-phase amplitudes are defined as $\hat{X} = \hat{a} + \hat{a}^\dagger$, $\hat{Y} = i(\hat{a}^\dagger - \hat{a})$, we have from Eq. (11)

$$\hat{X}_{1,2}^{(o)} = G\hat{X}_{1,2}^{(in)} + g\hat{X}_{2,1}^{(in)}, \quad \hat{Y}_{1,2}^{(o)} = G\hat{Y}_{1,2}^{(in)} - g\hat{Y}_{2,1}^{(in)}. \quad (12)$$

Note from the relation above that the output amplitudes are mixtures of the two input amplitudes, and thus, parametric amplifiers can act as beam splitters for wave splitting and mixing. The difference is that the outputs for parametric amplifiers are amplified because $G = \cosh r > 1$.

B. Interference fringe patterns

Assume that the input field \hat{a}_1^{in} is in a relatively strong coherent state $|\alpha\rangle$ ($|\alpha|^2 \gg 1$) and \hat{a}_2^{in} is in vacuum, and the fields in the two arms experience phase shifts of $\varphi_{1,2}$. Using Eq. (11) for the two parametric amplifiers, we find the output photon numbers as

$$I_1^{(o)} = |\alpha|^2 [G_1^2 G_2^2 + g_1^2 g_2^2 + 2G_1 G_2 g_1 g_2 \cos(\varphi_1 + \varphi_2)], \quad (13)$$

$$I_2^{(o)} = |\alpha|^2 [G_1^2 g_2^2 + G_2^2 g_1^2 + 2G_1 G_2 g_1 g_2 \cos(\varphi_1 + \varphi_2)],$$

where G_1 , g_1 and G_2 , g_2 are the amplitude gains of the two parametric amplifiers, respectively.

Comparing Eq. (13) to Eq. (1), we find three unique features that differentiate SU(1,1) interferometers [SU(1,1)] from Mach-Zehnder interferometers (MZI):

- The two outputs of SU(1,1) are in phase in contrast to 180° out of phase for MZI in Eq. (1).
- The interference fringes depend on the phase sum of φ_1 , φ_2 instead of the phase difference in MZI.
- The outputs are amplified when the gain parameters G_2 , g_2 are large.

The first property of in-phase fringes was demonstrated experimentally in the first realization of the SU(1,1) interferometer¹² and in the atom-light hybrid interferometer.⁵¹ This property leads to $I_1^{(o)} - I_2^{(o)} = |\alpha|^2$, which, unlike Eq. (3) of the traditional

MZI, is completely independent of the phase, making it impossible to obtain any phase change information in the intensity difference between the two outputs. This also indicates that the photon numbers of the two outputs are highly correlated, which is a property of parametric processes known as the Manley relation.⁵² The second property makes it impossible to have the common path rejection property in such devices as Sagnac interferometers but can give rise to signal enhancement when both beams are used to probe the phase change, as we will show in Sec. IV C. The third property leads to the enhancement of the signal size due to a small phase change δ in φ_2 of the probe field,

$$\begin{aligned}\delta I_1^{(o)} &= \delta I_2^{(o)} = 2\delta|\alpha|^2 G_1 G_2 g_1 g_2 \sin(\varphi_1 + \varphi_2) \\ &\approx 2G_2 g_2 I_{ps} \delta \sin(\varphi_1 + \varphi_2) \text{ for } g_1 \gg 1,\end{aligned}\quad (14)$$

where $I_{ps} \equiv g_1^2 |\alpha|^2 = I_2$. The enhancement factor is $G_2 g_2$ as compared to the MZI in Eq. (3) at the optimum condition of $R_1 \ll 1$, $T_2 = R_2 = 1/2$. This is because of the amplification of the second parametric amplifier when it mixes the two interfering fields.

C. Quantum noise performance of SU(1,1) interferometers

Although the signal due to the phase change is increased in SU(1,1) as compared to MZI, one may argue that this is not surprising at all because of the amplification of the second PA in SU(1,1). We can achieve the same effect if we place an amplifier at the outputs of the MZI. However, as we will see, there is a significant difference in the noise performance. An amplifier at the outputs of the MZI will amplify not only the signal but also the noise. So, the use of an amplifier at best keeps the signal-to-noise ratio. As a matter of fact, due to added noise from its internal degrees of freedom, such an amplifier often degrades the signal-to-noise ratio, leading to reduced measurement sensitivity.^{53–55} The SU(1,1), on the contrary, will not amplify the noise as much as the signal, leading to an enhancement of the signal-to-noise ratio. The key is in the destructive interference of the quantum noise, and it can be understood from the following three perspectives.

1. Quantum noise reduction by destructive quantum interference

Assume a coherent state $|\alpha\rangle$ input to the SU(1,1) and we make homodyne detection (HD) of $\hat{X}(\theta) = \hat{a}e^{-i\theta} + \hat{a}^\dagger e^{i\theta}$ at the outputs of PA2. It is straightforward to calculate the quantum fluctuations as¹¹

$$\begin{aligned}\langle \Delta^2 \hat{X}_1^{(o)}(\theta) \rangle &= \langle \Delta^2 \hat{X}_2^{(o)}(\theta) \rangle \\ &= |G_1 G_2 + g_1 g_2 e^{i(\varphi_1 + \varphi_2)}|^2 \\ &\quad + |G_1 g_2 + g_1 G_2 e^{i(\varphi_1 + \varphi_2)}|^2 \\ &= (G_1^2 + g_1^2)(G_2^2 + g_2^2) \\ &\quad + 4G_1 G_2 g_1 g_2 \cos(\varphi_1 + \varphi_2).\end{aligned}\quad (15)$$

The dependence on $\varphi_1 + \varphi_2$ is a result of quantum interference in SU(1,1), just as in the output photon numbers in Eq. (13). Although we find from Eq. (14) that the measured signal is maximum when $\varphi_1 + \varphi_2 = \pi/2$, the minimum noise is achieved at the dark fringe when $\varphi_1 + \varphi_2 = \pi$ and at balanced gain of $G_2 = G_1$, $g_2 = g_1$ for a given G_1, g_1 ,

$$\begin{aligned}\langle \Delta^2 \hat{X}_1^{(o)}(\theta) \rangle_m &= \langle \Delta^2 \hat{X}_2^{(o)}(\theta) \rangle_m \\ &= 1 + 2(G_1 g_2 - G_2 g_1)^2 \\ &= 1 \text{ when } G_1 = G_2, g_1 = g_2.\end{aligned}\quad (16)$$

Since the noise in each arm of the SU(1,1) after PA1 is $G_1^2 + g_1^2 = 1 + 2g_1^2 > 1$, the noise is reduced at the outputs of the SU(1,1) (PA2). This is because of the destructive quantum interference between the two arms that cancels the large quantum noise at each arm. Such a noise reduction effect was observed by Hudelist *et al.* in the first measurement of quantum noise performance of SU(1,1).¹³

Note that Eq. (16) is independent of the quadrature angle θ , which means that the noise is minimum for all quadrature-phase amplitudes $\hat{X}_{1,2}^{(o)}(\theta)$. This is quite different from squeezed state interferometry^{1–3} where only the squeezing quadrature has noise reduction. This indicates that the underlying physics for noise reduction here is quantum destructive interference, which reduces noise for the whole field including all quadrature-phase amplitudes, in contrast to the squeezed state interferometry where noise depends on the angle of quadrature-phase amplitudes.

2. Quantum beam splitter as a disentanglement tool

To understand how quantum interference occurs at PA2, we just need to recall Eq. (12), which shows the superposition of the quadrature-phase amplitudes of the incoming fields. Note that the relations are in quantum mechanical operator form, which means that quantum fluctuations or noise can be subtracted or added depending on the phase, giving rise to quantum interference. This shows that a parametric amplifier can act as a quantum beam splitter to split and mix waves. In this sense, the roles of a PA and a BS are the same in the mixing of waves: incoming waves are all superposed coherently. It is known that the two outputs of PA1 are entangled in the continuous variables of phases and amplitudes^{49,50} and two entangled fields can be transformed by a 50:50 beam splitter into two independent squeezed states with noise reduced at orthogonal quadratures.^{56–58} In this case, the BS acts as a disentangler that transforms two entangled fields into two unentangled fields. Since a PA and a BS are the same in wave mixing, the role of PA2 in the SU(1,1) interferometer is then a disentangler. This happens when the gains of PA1 and PA2 are equal, producing two unentangled fields at the outputs with noise at the vacuum level, as shown in Eq. (16).

On the other hand, the difference between a parametric amplifier (PA) and a linear beam splitter (BS) lies in the fact that a parametric amplifier (PA2) has amplified outputs. This feature can lead to the loss-tolerant property of SU(1,1) interferometers that we will discuss later in Sec. III E. It also leads to the following understanding.

3. Quantum noiseless amplification due to noise cancellation

The action of the SU(1,1) interferometer can be analyzed from another perspective, that is, quantum amplification. When viewed as an amplifier, one of the inputs of PA2 is regarded as the signal input, while the other input is treated as the internal mode of the amplifier.^{53–55} Normally, the internal mode of the amplifier is inaccessible from outside and is left in the vacuum state, which adds in vacuum noise to the amplified signal. This added noise is the extra

noise in addition to the input signal noise, leading to a degraded signal-to-noise ratio for the amplified signal compared to the input. If the internal mode can be accessed, as in the case of a parametric amplifier, squeezed states can be injected to it to reduce the extra added noise.^{54,55} This is the case when the input signal and the internal mode are uncorrelated. On the other hand, if the input signal and the internal mode are correlated, further noise reduction can be achieved. This was first studied by Ou⁵⁹ as early as in 1994 and was recently demonstrated⁶⁰ with an arrangement similar to an SU(1,1) interferometer. To understand this, we go back to the input–output relation in Eq. (12) for the parametric amplifier. We select field 1 as the signal field (*s*) and field 2 as the internal mode (*int*) and rewrite it as

$$\hat{X}_s^{(o)} = G\hat{X}_s^{(in)} + g\hat{X}_{int}^{(in)}. \quad (17)$$

If the signal and internal modes are independent, we have

$$\langle \Delta^2 \hat{X}_s^{(o)} \rangle = G^2 \langle \Delta^2 \hat{X}_s^{(in)} \rangle + g^2 \langle \Delta^2 \hat{X}_{int}^{(in)} \rangle. \quad (18)$$

The second term in the expression above is the extra noise for the output that degrades the output SNR as compared to the input. However, if the input signal and the internal modes are correlated, we have from Eq. (17)

$$\langle \Delta^2 \hat{X}_s^{(o)} \rangle = G^2 \langle \Delta^2 (\hat{X}_s^{(in)} + \lambda \hat{X}_{int}^{(in)}) \rangle, \quad (19)$$

with $\lambda \equiv g/G$. If the signal and the internal modes are in the EPR-type entangled state such as those generated from the first PA, $\hat{X}_s^{(in)}$ and $\hat{X}_{int}^{(in)}$ are quantum mechanically correlated so that $\langle \Delta^2 (\hat{X}_s^{(in)} + \lambda \hat{X}_{int}^{(in)}) \rangle$ can be smaller than the corresponding vacuum value of $1 + \lambda^2$. In fact, it was shown⁵⁹ that noiseless quantum amplification can be achieved with the proper adjustment of the parameter. Such an effect of noise reduction in amplifiers due to entanglement was demonstrated first by Kong *et al.*⁶⁰ in an atomic vapor system and later by Guo *et al.*¹⁷ in a nonlinear fiber amplifier.

D. Signal-to-noise ratio and the optimum phase measurement sensitivity in SU(1,1) interferometers

The sensitivity of SU(1,1) interferometers for phase measurement is determined not only by the noise level of the outputs but also by the signal size due to the phase change. It is usually characterized by the signal-to-noise ratio (SNR), especially in experiment. Although the signal size due to the phase change is usually the best at half of the fringe size, i.e., the overall phase is at $\pi/2$, it is better to operate at the dark fringe for practical reasons, similar to the Mach–Zehnder interferometer in Sec. II, and we make homodyne measurement of $\hat{Y} = i(\hat{a}^\dagger - \hat{a})$. Referring to Fig. 3, when input field 1 to the interferometer is in a strong coherent state of $|\alpha\rangle$ and the overall phase $\varphi_1 + \varphi_2$ is set at π for minimum at both outputs, we obtain the signals at the two outputs for a small phase change δ in one arm of the interferometer,⁶¹

$$\langle \hat{Y}_1^{(o)} \rangle = 2g_1g_2|\alpha|\delta, \quad \langle \hat{Y}_2^{(o)} \rangle = 2g_1G_2|\alpha|\delta. \quad (20)$$

With the output noise given in Eq. (15), we obtain the SNRs at the two outputs as

$$\begin{aligned} \text{SNR}_{SU(1,1)}^{(1)} &= \frac{\langle \hat{Y}_1^{(o)} \rangle^2}{\langle \Delta^2 \hat{Y}_1^{(o)} \rangle} \\ &= \frac{4g_2^2g_1^2|\alpha|^2\delta^2}{(G_1^2 + g_1^2)(G_2^2 + g_2^2) - 4G_1G_2g_1g_2} \\ &= \frac{4g_2^2I_{ps}\delta^2}{(G_1^2 + g_1^2)(G_2^2 + g_2^2) - 4G_1G_2g_1g_2} \end{aligned} \quad (21)$$

and

$$\begin{aligned} \text{SNR}_{SU(1,1)}^{(2)} &= \frac{4G_2^2g_1^2|\alpha|^2\delta^2}{(G_1^2 + g_1^2)(G_2^2 + g_2^2) - 4G_1G_2g_1g_2} \\ &= \frac{4G_2^2I_{ps}\delta^2}{(G_1^2 + g_1^2)(G_2^2 + g_2^2) - 4G_1G_2g_1g_2}, \end{aligned} \quad (22)$$

where $I_{ps} = g_1^2|\alpha|^2$ is the photon number of the phase sensing field. When $g_2 > g_1$ and $g_2 \gg 1$ so that $G_2^2 = 1 + g_2^2 \approx g_2^2$, the SNR takes the maximum value of⁶¹

$$\text{SNR}_{SU(1,1)}^{(1,2)op} = 2(G_1 + g_1)^2 I_{ps} \delta^2, \quad (23)$$

which gives $\delta_m^{SU(1,1)} = \sqrt{2}\delta_m / (G_1 + g_1)$ when $\text{SNR}_{SU(1,1)}^{(1,2)op} = 1$.

Note that the optimum SNR is obtained not with equal gains of the two PAs but under the condition of $g_2 > g_1$, $g_2 \gg 1$.⁶² The former was the operational condition commonly used in earlier discussions^{7,8,10,11} and experimental realizations of SU(1,1)^{12,13} and corresponds to the minimum noise level at the outputs, as shown in Eq. (16). However, it leads to an SNR of $(G_1 + g_1)^2 I_{ps} \delta^2$, which is a factor of 2 smaller than the optimum value given in Eq. (23).⁶¹

Comparing Eq. (23) to the optimum classical SNR in Eq. (7), we obtain an SNR enhancement factor of $(G_1 + g_1)^2/2$. This is a factor of 2 smaller than that of the squeezed state interferometry given in Eq. (9). The reason for this is related to the optimum scheme of SU(1,1) for phase measurement and will be discussed later in Sec. IV C.

Figure 4 shows a typical result of phase measurement by both an SU(1,1) interferometer (red, SU11) and a Mach–Zehnder interferometer (black, MZ) under the condition of the same phase sensing intensity.⁶³ The peaks are the phase modulation signal, and the

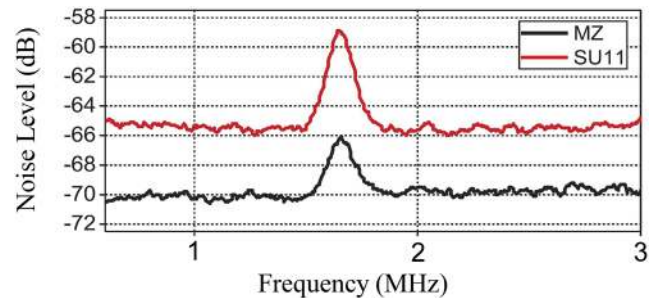


FIG. 4. Phase modulation signals and noise levels for an SU(1,1) interferometer (red) and a Mach Zehnder interferometer (black). Adapted with permission from Du *et al.*, Opt Lett. **43**, 1051 (2018). Copyright 2018 Optical Society of America.

flat floor is the noise level of measurement. As can be seen, both the signal and noise are amplified for SU(1,1) as compared to MZI, but the signal gain is more than noise gain. We can extract SNRs from Fig. 4. Since it is in log-scale, the SNR of phase measurement is simply the difference of the peak value and the floor value. It is found that $\text{SNR}_{\text{SU}(1,1)} = 6.9$ dB and $\text{SNR}_{\text{MZI}} = 3.9$ dB, leading to an improvement of 3.0 dB in SNR by SU(1,1) over MZI.

Since both outputs of PA2 contain the information about the phase change, it is suggested^{15,43} to measure the joint quantity $\hat{Y}_{JM} \equiv \hat{Y}_1^{(o)} + \hat{Y}_2^{(o)}$ to combine the information. It is straightforward to show⁶¹ that in this case, the SNR is independent of g_2 and has the optimum value given in Eq. (23), $\text{SNR}_{JM} = \text{SNR}_{\text{SU}(1,1)}^{(1,2)op} = 2(G_1 + g_1)^2 I_{ps} \delta^2$, but with no further improvement. The extra output nonetheless can be used for quantum information tapping (see Sec. VI C and Ref. 17).

It should be noted that the SNR enhancement of SU(1,1) interferometers over the classical SNR is due to the employment of parametric amplifiers, which require strong pumping for high gain and thus consume more energy or resources than traditional interferometers.

E. Effect of losses

It is well known that with some loss L such as detection inefficiency involved in the squeezed state, the noise reduction effect is degraded with Eq. (8) modified to

$$\langle \Delta^2 I_{-}^{sq} \rangle = |\alpha|^2 [(1-L)e^{-2r} + L], \quad (24)$$

where the loss L is modeled as a beam splitter with a transmissivity of $1-L$. The above can be considered as contributions from two parts: the transmitted squeezed noise $|\alpha|^2 e^{-2r}$ with a probability of $1-L$ and the vacuum noise of size $|\alpha|^2$ reflected from the unused port with a probability of L , all scaled to the shot noise level of $\langle \Delta^2 I_{-}^{sq} \rangle = |\alpha|^2$. Note that in the existence of loss L , the best noise reduction achievable is L at infinite squeezing ($r \rightarrow \infty$). After considering the reduction of the signal due to loss, we arrive at the best SNR enhancement factor as $(1-L)/L$ for the squeezed state interferometry.

On the other hand, the output noise for the SU(1,1) is amplified by the second PA, making it much larger than the vacuum noise level so that the extra noise coupled in through loss is negligible. This is shown in Eq. (15), which becomes

$$\begin{aligned} \langle \Delta^2 \hat{X}_1^{(o)}(\theta) \rangle &= \langle \Delta^2 \hat{X}_2^{(o)}(\theta) \rangle \\ &= (G_1^2 + g_1^2)(G_2^2 + g_2^2) - 4G_1 G_2 g_1 g_2 \\ &= 1 + 2(G_1 g_2 - G_2 g_1)^2 \\ &\gg 1 \text{ for } G_2 \gg G_1 > 1 \end{aligned} \quad (25)$$

at dark fringe when $\varphi_1 + \varphi_2 = \pi$. So, the noise for $\hat{Y}_1^{(o)}$ after the loss L is

$$\begin{aligned} \langle \Delta^2 \hat{Y}_1^{(o)} \rangle_L &= (1-L) \langle \Delta^2 \hat{Y}_1^{(o)} \rangle + L \\ &\approx (1-L) \langle \Delta^2 \hat{Y}_1^{(o)} \rangle. \end{aligned} \quad (26)$$

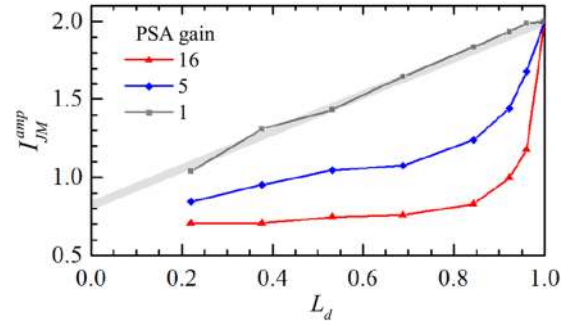


FIG. 5. Dependence of the measured quantum noise level I_{JM}^{amp} as a function for the detection losses for various gain of the parametric amplifier (PSA gain). The value of 2 corresponds to the vacuum noise level. Reproduced with permission from Li *et al.*, Opt. Express **27**, 30552 (2019). Copyright 2019 Optical Society of America.

With the signal drop by a factor of $1-L$, $\langle \hat{Y}_1^{(o)} \rangle_L^2 = (1-L) \langle \hat{Y}_1^{(o)} \rangle^2$, we obtain the SNR due to loss,

$$\text{SNR}_{\text{SU}(1,1)}^L = \frac{\langle \hat{Y}_1^{(o)} \rangle_L^2}{\langle \Delta^2 \hat{Y}_1^{(o)} \rangle_L} \approx \frac{\langle \hat{Y}_1^{(o)} \rangle^2}{\langle \Delta^2 \hat{Y}_1^{(o)} \rangle} = \text{SNR}_{\text{SU}(1,1)}. \quad (27)$$

So, the losses outside of the interferometer such as transmission and detection losses have almost no effect on the SNR of SU(1,1) for large G_2 and the ability of loss tolerance increases with G_2 of PA2.^{11,61} This loss-tolerant property of SU(1,1) was first observed in Ref. 13 and confirmed later in Refs. 16 and 64. Figure 5 shows the result from Ref. 64, which plots the measured quantum noise level I_{JM}^{amp} (value of 2 corresponds to the vacuum level) as a function of loss for various gain of the parametric amplifier (PA2). It clearly demonstrates that the effect of loss is mitigated by the amplification (PSA gain). The gray straight line (PSA gain = 1) corresponds to the case of direct detection and is described by the linear dependence in Eq. (24).

In fact, the amplified quantum noise from PA2 can not only overcome the vacuum noise introduced through losses, but it can also fight against excess classical noise. This strategy was used in microwave detection to tackle the enormous thermal noise background in a microwave circuit⁶⁵ (see Sec. V A).

SU(1,1)'s immunity to losses is only for the output fields of the SU(1,1). For losses inside the interferometer, however, it was shown^{11,66} that the effect is exactly the same as that on the squeezed state. So, SU(1,1) is not immune to its internal losses. This suggests that all the quantum advantage is from the quantum entanglement created in the first PA (PA1), whereas the second PA is simply a device for superposition to disentangle the two fields in the two arms of the interferometer.

Indeed, as variations of SU(1,1), we can replace the second PA with any linear device that can mix the two fields and achieve the same performance as SU(1,1), as we will see in the following.

IV. VARIATIONS OF SU(1,1) INTERFEROMETERS

A. The Scheme of a parametric amplifier and a beam splitter (PA + BS)

It has been known almost since the discovery of squeezed states and EPR-entangled states that in the case of degenerate frequency,

they can be converted from each other by a 50:50 beam splitter.^{56,67} Since an EPR-type entangled state can be generated with a parametric amplifier,⁵⁰ we can use a beam splitter to convert it to squeezed states and measure the phase change with reduced quantum noise, similar to the squeezed state interferometry. However, the statements above are for states with no coherent components and the photon number of squeezed states with no coherent component is too low to have any practical use.

To boost the photon number, we can inject a coherent state, just like what we did in Sec. III. This forms a variation of the SU(1,1) interferometer with a PA for beam splitting and a BS for wave superposition and interference (PA + BS scheme). The actual scheme is shown in Fig. 6. For a large injection $|\alpha|^2 \gg 1$, it is straightforward to calculate⁵⁸ the output intensity at output port 2 as

$$I_2^{(o)} = I_{ps}[1 - \mathcal{V}\cos(\varphi_1 + \varphi_2)], \quad (28)$$

where $I_{ps} = g_1^2|\alpha|^2$ and visibility $\mathcal{V} \equiv 2G_1g_1\sqrt{TR}/(g_1^2 + R)$. Note that the fringe depends on the sum of the phases of the two arms, similar to Eq. (13). 100% visibility in interference fringe at output port 2 can be achieved with $T = G_1^2/(G_1^2 + g_1^2)$, $R = 1 - T$ for the beam splitter. However, when $\hat{Y}_2^{(o)}$ is measured at output port 2 by homodyne detection (HD), the optimum SNR for phase measurement is achieved when $T = (G_1^2 + g_1^2)^2/(8G_1^2g_1^2 + 1)$, $R = 4G_1^2g_1^2/(8G_1^2g_1^2 + 1)$ with

$$\text{SNR}_{PA+BS}^{(op)} = 4\delta^2 I_{ps}(G_1^2 + g_1^2). \quad (29)$$

This is a factor of $G_1^2 + g_1^2$ improvement over the optimum classical SNR in Eq. (7).

If we use a 50:50 beam splitter, as in Ref. 56, it is straightforward to find that the output noise will be $(G_1 - g_1)^2$, while the signal is $2I_{ps}\delta^2$, and the SNR is exactly the same as that in Eq. (23). So, this variation of SU(1,1) gives the same SNR improvement factor as the SU(1,1) over the traditional interferometer. It is interesting to note if we switch the positions of PA and BS, that is, using BS for beam splitting and PA for wave superposition, the result will not be that given in Eq. (29) but is the same as that in Eq. (7) for classical interferometers.⁵⁸ This further demonstrates that the quantum advantage originates from the quantum entanglement in the phase probing beam produced by the first parametric amplifier. Note further that since we use a BS to superpose the signal and idler fields,

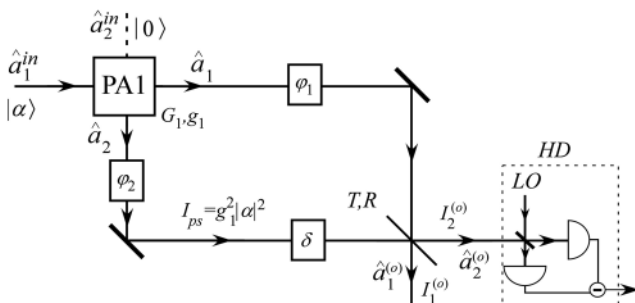


FIG. 6. The scheme of the parametric amplifier and beam splitter for a variation of the SU(1,1) interferometer. Adapted with permission from J. Kong, Z. Y. Ou, and W. Zhang, Phys. Rev. A **87**, 023825 (2013). Copyright 2013 American Physical Society.

they must be frequency degenerate and the scheme is sensitive to losses just like squeezed state interferometry.

B. Truncated SU(1,1) interferometer

Although waves need to be superimposed in order to show the interference effect, the method of superposition can vary. We have already seen the methods using a parametric amplifier and using a beam splitter. In these cases, the waves are physically superimposed and interference occurs at the optical fields of the outputs of the wave-combining devices. In particular, for the PA + BS scheme in Fig. 6, it requires the two fields from PA1 have the same frequency because of the use of the beam splitter for wave superposition. On the other hand, since homodyne detection makes quantum measurement of the quadrature-phase amplitude of the field, the photo-current from homodyne detection can be thought of as the quantum copy of the amplitude of the field. So, the mixing of the photo-currents after homodyne detections is equivalent to the superposition of the detected fields and we can replace the beam splitter with a post-detection current mixer to achieve field superposition. This is the idea behind the so-called “truncated” SU(1,1) interferometer proposed and reported by Anderson *et al.*,^{15,43} as shown in Fig. 7 where only the first parametric amplifier remains as compared to SU(1,1) interferometers in Figs. 1(b) and 6. The mixer for photo-currents from the homodyne detectors (HD) plays the same role as the second parametric amplifier in Fig. 1(b) and the beam splitter in Fig. 6 to superimpose the two fields in the interferometer for interference. The current after mixing shows the phase signal $\delta\phi$ as well as the quantum noise cancellation effect due to entanglement in a typical SU(1,1) interferometer. It was shown^{43,61} that the SNR for phase measurement is the same as that in Eq. (23) in the ideal lossless condition. The truncated version of SU(1,1) was recently used in atomic force microscopy with quantum enhancement.⁶⁸

Because direct detection is used in the truncated scheme and the PA + BS scheme of SU(1,1) interferometers, losses will have a significant effect on the quantum enhancement factor in a similar way to the squeezed state interferometry.

C. Dual-beam SU(1,1) interferometers

In the SU(1,1) interferometers we discussed so far, the SNR for phase measurement is given in Eq. (23), which shows an improvement factor of $(G_1 + g_1)^2/2$ over the optimum classical SNR in Eq. (7). This is a factor of 2 smaller than the improvement factor

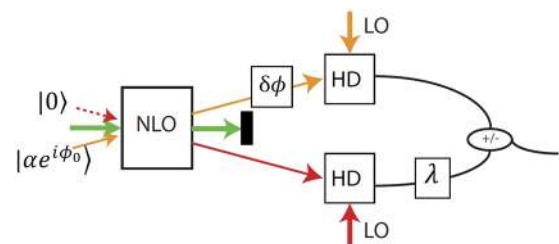


FIG. 7. The scheme of the truncated SU(1,1) interferometer. Reproduced with permission from Gupta *et al.*, Opt. Express **26**, 391 (2018). Copyright 2018 Optical Society of America.

by squeezed state interferometry given in Eq. (9). The reason for this is quantum resource sharing in phase and amplitude measurement,⁶¹ which will be discussed later in Sec. VI B. This means that the current SU(1,1) interferometer is not optimized for phase measurement. To look for the optimized phase measurement scheme, we note in Eqs. (13) and (28) that the interference fringe depends on the sum of the phases of the two arms of the interferometer. Therefore, if we use both fields from PA1 to sense the phase change signal, we will double the signal size δ . This is the dual-beam scheme proposed by Li *et al.*⁶¹ and realized by Liu *et al.*,⁶⁹ which is shown in Fig. 8. As expected, it can be shown⁶¹ that the homodyne detection signals at both output ports are

$$\begin{aligned}\langle \hat{Y}_1 \rangle^2 &= 4(G_1 G_2 + g_1 g_2)^2 |\alpha|^2 \delta^2, \\ \langle \hat{Y}_2 \rangle^2 &= 4(G_1 g_2 + g_1 G_2)^2 |\alpha|^2 \delta^2.\end{aligned}\quad (30)$$

With the noise power given in Eq. (15) [quantities $\hat{X}_{1,2}^{(o)}(\pi/2)$ are the same as $\hat{Y}_{1,2}$ here] and at the dark fringe of $\varphi_1 + \varphi_2 = \pi$, the SNR for the dual-beam scheme is

$$\begin{aligned}\text{SNR}_{DB}^{(1)} &= \frac{4(G_1 G_2 + g_1 g_2)^2 I_{ps} \delta^2}{(G_1^2 + g_1^2)[(G_1^2 + g_1^2)(G_2^2 + g_2^2) - 4G_1 G_2 g_1 g_2]}, \\ \text{SNR}_{DB}^{(2)} &= \frac{4(G_1 g_2 + g_1 G_2)^2 I_{ps} \delta^2}{(G_1^2 + g_1^2)[(G_1^2 + g_1^2)(G_2^2 + g_2^2) - 4G_1 G_2 g_1 g_2]},\end{aligned}\quad (31)$$

where $I_{ps} = (G_1^2 + g_1^2)|\alpha|^2$ is the photon number of the dual phase sensing fields. When $g_2 \rightarrow \infty$ and $G_2 \approx g_2$, we have the optimum SNR,

$$\begin{aligned}\text{SNR}_{DB}^{(1)} &= \text{SNR}_{DB}^{(2)} = 2(G_1 + g_1)^4 I_{ps} \delta^2 / (G_1^2 + g_1^2) \\ &\rightarrow 4(G_1 + g_1)^2 I_{ps} \delta^2 \text{ for } g_1 \gg 1,\end{aligned}\quad (32)$$

which is the same as the one for squeezed state interferometry in Eq. (9) at large g_1 .

Note that at finite g_1 , the SNR in Eq. (32) is still smaller than that for squeezed state interferometry. This is again because of quantum resource distribution, which we will discuss in Sec. VI B. Note that the SNRs in Eq. (31) are for one output only, but we have two outputs for PA2. So, we can make full use of these two outputs by performing a joint measurement $\hat{Y}_{JM} \equiv \hat{Y}_1 + \lambda \hat{Y}_2$ of the two outputs, as shown in Fig. 8. With $\lambda = 1$ and any g_2 , it is shown that the SNR for the joint measurement is

$$\text{SNR}_{DB}^{JM} = 4(G_1 + g_1)^2 I_{ps} \delta^2 \text{ for arbitrary } g_1. \quad (33)$$

So, we recover the SNR of squeezed state interferometry when we make full use of the resource.

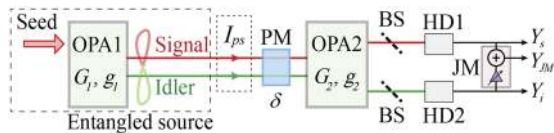


FIG. 8. The dual-beam scheme of the SU(1,1) interferometer for phase measurement. Reproduced with permission from Liu *et al.*, Opt. Express **27**, 11292 (2019). Copyright 2019 Optical Society of America.

From the result above, we find that SU(1,1) at best matches the sensitivity of squeezed state interferometry. This seems to contradict the fact that SU(1,1) can reach the Heisenberg limit of phase measurement.⁷ However, the result in Eq. (33) is obtained under the condition of strong coherent state injection to boost overall phase sensing photon number I_{ps} . With no coherent state injection, it was shown¹¹ that the Heisenberg limit is recovered. It was further shown⁵⁸ that when the gain parameter g_1 of PA1 is comparable to the injected coherent state photon number, the Heisenberg limit can also be reached, similar to squeezed state interferometry.^{47,48}

It was shown⁶¹ that when dual-beam phase sensing is implemented in the truncated scheme and the PA + BS scheme, the factor of 2 is also recovered, leading to the same SNR as the squeezed state interferometry. However, because of the second PA, the dual-beam SU(1,1) scheme here is tolerant to losses outside of the interferometer, similar to the original SU(1,1) interferometer in Fig. 3. Furthermore, different from the PA + BS scheme, the employment of separate homodyne detectors in the truncated scheme and the second PA in the dual-beam SU(1,1) scheme does not require the same frequency for the two fields from the first PA in both schemes. The experimental implementation of the dual-beam SU(1,1) interferometer was realized by Liu *et al.*,⁶⁹ and about 3 dB improvement over the single-beam scheme was demonstrated.

D. Multi-stage SU(1,1) interferometers

Similar to multi-path interferometers such as Fabry–Perot interferometers and multi-slit interference in optics, we can also add more PAs to form multi-stage SU(1,1) interferometers. In order to have all the PAs playing the same role in the multi-path interference, we usually work at a low gain regime of the PAs so that spontaneous emission dominates and two-photon states are generated. This variation of the SU(1,1) interferometer finds its application in the modification of mode structures (temporal and spatial) in the output field for mode engineering of the output quantum states. The detail of this application can be found later in Sec. VI E. In the following, we will present the general principle for this scheme.

Consider the multi-stage interferometer shown in Fig. 9 where the k th PA is described by the small amplitude gain parameter $0 < g_k \ll 1$ so that the power gain $G_k^2 = 1 + g_k^2 \approx 1$ ($k = 1, 2, \dots, N$). In between the PAs sandwiched are phase shifters $\hat{\Theta}(\theta)$. For simplicity, we assume the phase shifters have the same phase of the amount θ for the two fields of the PAs together. In the low gain limit, in order to better describe the performance of the system and reveal the underlying physical principle, we will work in the Schrödinger picture with quantum states. Let us start with the quantum state of one PA.

With the Hamiltonian in Eq. (10) for the parametric amplifier, the state evolution in the time interval Δt for the system is described

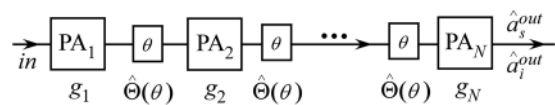


FIG. 9. Multi-stage SU(1,1) interferometer.

by a unitary evolution operator,

$$\begin{aligned}\hat{U}(\Delta t) &= \exp(\hat{H}\Delta t/i\hbar) \\ &\approx 1 + (g\hat{a}_s^\dagger\hat{a}_i^\dagger + h.c.) \text{ when } g \equiv \xi\Delta t \ll 1,\end{aligned}\quad (34)$$

where we replace the labeling of the fields in Eq. (10) by s, i , which stand for “signal, idler” due to historic reason, and assume $g \equiv \xi\Delta t$ is a positive number and only keep the first order in the expansion of the exponential. Then, with vacuum input, the output state is a two-photon state of the form

$$\begin{aligned}|\Psi\rangle_{PA} &= \hat{U}(t)|vac\rangle \approx |vac\rangle + g\hat{a}_s^\dagger\hat{a}_i^\dagger|vac\rangle \\ &= |vac\rangle + g|1_s, 1_i\rangle.\end{aligned}\quad (35)$$

For the multi-stage interferometer in Fig. 9, the output state is then

$$\begin{aligned}|\Psi\rangle_{mPA} &= \hat{U}_N(\Delta t)\hat{\Theta}(\theta)\cdots\hat{U}_2(\Delta t)\hat{\Theta}(\theta)\hat{U}_1(\Delta t)|vac\rangle \\ &\approx |vac\rangle + \left(\sum_{k=1}^N g_k e^{-i(N-k)\theta}\right)|1_s, 1_i\rangle,\end{aligned}\quad (36)$$

where the operator $\hat{\Theta}(\theta)$ adds a total phase of θ to the signal and idler field together. So, the multi-stage interferometer is equivalent to one PA but with amplitude gain equal to the sum of the amplitude gains of all PAs involved: $g_T = \sum_{k=1}^N g_k e^{-i(N-k)\theta}$. This is the result of two-photon interference: each PA can generate a pair of photons with amplitude g_k , and the final state is a superposition of all the two-photon states.

In the special case when all the PAs have the same gain, $g_k = g$, we have

$$g_T = g \sum_{k=1}^N e^{-i(k-1)\theta} = g e^{-i(N-1)\theta/2} H(\theta), \quad (37)$$

where $H(\theta) \equiv \frac{\sin N\theta/2}{\sin \theta/2}$ is the multi-path interference factor, which recovers the familiar function of $\cos \theta$ for $N = 2$. It first appears in multi-slit interference such as optical grating and has an enhancement factor of N^2 for the two-photon production rate as compared to the single PA. This is the same physics underlying cavity enhanced parametric processes⁷⁰ and can provide active filtering for spectral mode shaping (see Sec. VI E for details).

The high gain case is not easy to treat because of the general non-commuting nature of the Hamiltonian for different PAs.⁷¹ Nevertheless, it still gives rise to the modification of the mode structure at the output similar to the low gain case.

V. SU(1,1) INTERFEROMETERS OF DIFFERENT WAVES

A. SU(1,1) interferometer with microwaves

Parametric amplifiers were first realized in radio frequency and microwaves.⁷² However, thermal and electronic noise is often so large that it overwhelms the quantum noise in detection processes. So, it is hard to study the quantum behavior of the amplifiers in radio frequency and microwave regimes. This was changed recently when near quantum limit low noise parametric amplifiers were invented.⁷³ Although thermal and electronic noise is still very high in detection processes, Flurin *et al.*⁶⁵ utilized the low noise parametric amplifier at high gain as a beam splitter to reveal the EPR-type quantum correlation between two entangled microwave fields generated by another

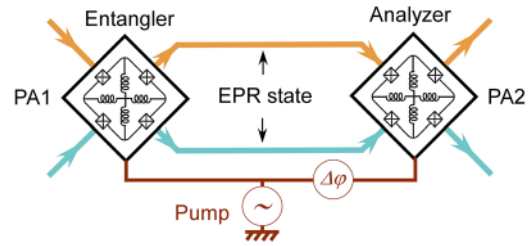


FIG. 10. SU(1,1) interferometer for microwaves. Adapted with permission from Flurin *et al.*, Phys. Rev. Lett. **109**, 183901 (2012). Copyright 2012 American Physical Society.

low noise parametric amplifier. Similar to the role played for loss tolerance by the second parametric amplifier in an SU(1,1) interferometer, Flurin *et al.*⁶⁵ used the low noise parametric amplifier to amplify the quantum noise to a level that is much larger than the thermal and electronic background noise in the detection process. In this way, they achieved the measurement of the correlated quantum noise from EPR-entangled microwave fields even in the presence of the enormous thermal and electronic background noise.

Working on the goal to demonstrate the EPR-type entanglement between microwave fields, Flurin *et al.*⁶⁵ inadvertently realized an SU(1,1) interferometer in the microwave regime. In their arrangement shown in Fig. 10, the first amplifier (PA1) is the EPR-entangled source (entangler), while the second one (PA2) is the one that measures the entanglement (analyzer). This geometry is exactly in the form of Fig. 3 and is an SU(1,1) interferometer but without seeding of a coherent state. Indeed, the measurement result shows an interference pattern that depends on the phase difference $\Delta\phi$ of the pumps.⁶⁵ Note that during the experiment described in Ref. 65, the gain of the analyzer (PA2) is much larger than 1 and is always larger than that of the entangler (PA1). This is exactly the setting for achieving the optimum performance of the SU(1,1) interferometer presented in Eq. (23). The large gain in the analyzer (PA2) also satisfies what is required for PA2 to act as an entanglement measurement device (see more later in Sec. VI D and Ref. 64).

B. Atom-light hybrid interferometers

One of the key differences of an SU(1,1) interferometer from a traditional interferometer is the way of wave splitting and superposition for interference: it is through nonlinear mixing of waves. This method can therefore couple different types of waves for interference, which is basically impossible in a traditional interferometer. This leads to hybrid interferometers where the two interfering waves are different types of waves. One such interferometer is the atom-light hybrid interferometer, first realized by Chen *et al.* in 2015.⁵¹

Similar to the all-optical SU(1,1) interferometer in the original realizations,^{12,13} the wave splitting and superposition elements in an atom-light hybrid interferometer are Raman amplifiers, which are a special kind of parametric process. As shown in the inset of Fig. 11, a Raman process couples light waves of strong Raman pump field A_W and Stokes field \hat{a}_S with an atomic collective excitation wave \hat{S}_a (also known as a pseudo-spin wave) between two lower states (g, m) via

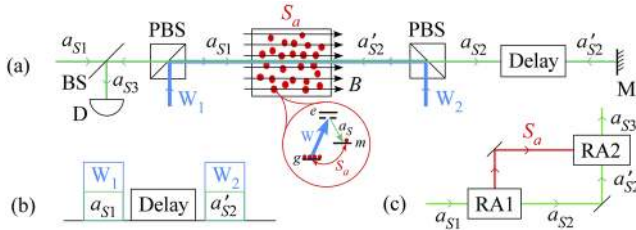


FIG. 11. Hybrid atom-light interferometers. (a) Schematic diagram of the interferometer; PBS: polarization beam splitter, BS: beam splitter, M: mirror, D: detector, B: magnetic field for atomic phase change. (b) Time sequence of light pulses. (c) MZ interferometer-equivalent interference paths for atomic spin wave S_a and optical wave a_S , RA1, RA2: Raman amplifiers. Inset: atomic levels and optical waves.

an excited state (e). The Raman interaction Hamiltonian^{74,75} has the same form as the parametric interaction Hamiltonian in Eq. (10),

$$\hat{H}_R = i\hbar\eta A_W \hat{a}_S^\dagger \hat{S}_a^\dagger - i\hbar\eta^* A_W^* \hat{a}_S \hat{S}_a, \quad (38)$$

except that one of the light fields, say \hat{a}_2 , is replaced by the atomic spin wave \hat{S}_a and the other field \hat{a}_1 is renamed as the Stokes field \hat{a}_S .

In most applications of Raman amplifiers, the atomic states are treated as inaccessible internal states of the amplifier, which are often in the vacuum state (unexcited state) and are not taken into consideration. They are responsible for the spontaneous emission noise of the amplifier. For the action of the SU(1,1) interferometer, as we see from Sec. III, it requires the atomic spin wave to participate as one of the interfering fields. Therefore, the atomic spin wave is a part of the waves participating in the interference together with the optical Stokes field. So, the interference fringe will depend on both the atomic phase and the optical phase, thus forming an atom-light hybrid SU(1,1) interferometer. The schematic diagram is shown in Fig. 11(a). The input Stokes field a_{S1} , after interacting with atoms pumped by the first writing field W_1 [see Fig. 11(b) for the time sequence], is amplified as a_{S2} . In the meantime, an atomic spin wave S_a is also generated in the atomic ensemble. This is the wave splitting process [RA1 in Fig. 11(c)]. Since the atomic spin wave stays in the atomic ensemble, to combine it with the amplified Stokes, we send back with a mirror (M) the delayed Stokes field a'_{S2} together with the second write field W_2 [RA2 in Fig. 11(c); see Fig. 11(b) for the time sequence]. This design is somewhat similar to a Michelson interferometer where one BS is used for dual purpose.¹⁴ The output a_{S3} is detected by D to reveal the interference fringe as the optical or atomic phase is scanned. The atomic phase can be changed by the external magnetic field via the Zeeman effect, as demonstrated by Chen *et al.*⁵¹

The atomic phase can also be altered by shining an off-resonant light beam on the atoms via the AC Stark shift.⁷⁶ Thus, an interesting application of the atom-light interferometer is to measure the photon number of the off-resonant light field in the sense of quantum non-demolition (QND) measurement.⁷⁷ This approach is similar to the QND measurement scheme for microwave photons.⁷⁸

C. Atomic SU(1,1) interferometer

The atomic interferometer discussed in Sec. V B is a hybrid version involving optical waves in interference. An all-atom version of

the SU(1,1) interferometer in a spinor Bose–Einstein condensate was first discussed by Gabbriellini *et al.*⁷⁹ and experimentally realized by Linnemann *et al.*⁸⁰ This subject was covered in an excellent review by Pezzé *et al.*⁸¹ The nonlinear interaction responsible for atomic wave splitting and superposition is the spin exchange collision between ⁸⁷Rb atoms of spin $F = 2$ manifold and has a Hamiltonian of the form similar to Eq. (10) for the parametric process,

$$\hat{H}_{at} = \hbar\kappa \hat{a}_\uparrow^\dagger \hat{a}_\downarrow^\dagger + H.c., \quad (39)$$

where $\hat{a}_\uparrow, \hat{a}_\downarrow$ correspond to the atomic fields in the spin states of $|\uparrow\rangle \equiv |F = 2, m_F = 1\rangle$ and $|\downarrow\rangle \equiv |F = 2, m_F = -1\rangle$, respectively. The effective nonlinear coupling $\kappa \equiv gN_0$ is related to the microscopic nonlinearity g , arising from coherent collisional interactions and the number of colliding atoms N_0 in the initial state of $|F = 2, m_F = 0\rangle$, acting as the pump mode. Figure 12 shows the schematic of the interferometer (a) and the phase-dependent atomic numbers with their average showing the interference pattern (b). Note that the sum of the two output channels is measured because they are in phase, which is the unique property of the SU(1,1) interferometer. This version of the SU(1,1) interferometer is the unseeded one without coherent state injection since initially there is no atom in either $|\uparrow\rangle$ or $|\downarrow\rangle$ state. Nonetheless, phase measurement sensitivity beyond the SQL was demonstrated.

The atom-light hybrid interferometer discussed in Sec. V B and the atomic SU(1,1) interferometers discussed here all involve atomic internal states. An atomic interferometer usually refers to interferometers involving the de Broglie matter waves of atoms via their external motional states.⁸² An SU(1,1) of this type requires matter wave amplifiers,^{83,84} which can be realized by four-wave mixing of matter waves.⁸⁵

For the hybrid atom-light interferometer involving the external translational degrees of freedom of atoms, we need to go back to Raman amplification but deal with ultra-cold atoms in a BEC^{86–88} where super-radiance of light is correlated with the atomic motional states in a similar way as in Eq. (38).

D. Phonon SU(1,1) interferometer

Parametric amplifiers are the essential ingredients for an SU(1,1) interferometer. Nonlinear interactions are usually involved for them as we have seen before in Raman amplifiers and parametric processes. Opto-mechanical systems couple light fields with a mechanical oscillator and can realize similar nonlinear interaction for parametric amplification. The opto-mechanical coupling between a mechanical oscillator and a single optical cavity mode has an interaction Hamiltonian given by⁸⁹

$$\hat{H}_{OM} = \hbar\gamma \hat{a}^\dagger \hat{a} \hat{x}_m, \quad (40)$$

where $\hat{x}_m = \hat{b} + \hat{b}^\dagger$, \hat{a} and \hat{b} are the annihilation operators for the optical cavity mode and the phonon mode of the mechanical oscillator, respectively, and γ is the opto-mechanical coupling constant. With a strong coherent optical field, we can make a linear approximation $\hat{a} = \alpha + \hat{a}_s$, and the Hamiltonian in Eq. (40) becomes

$$\hat{H}_{OM} \approx \hbar\Gamma(\hat{a}_s^\dagger \hat{b} + h.c.) + \hbar\Gamma(\hat{a}_s^\dagger \hat{b}^\dagger + h.c.), \quad (41)$$

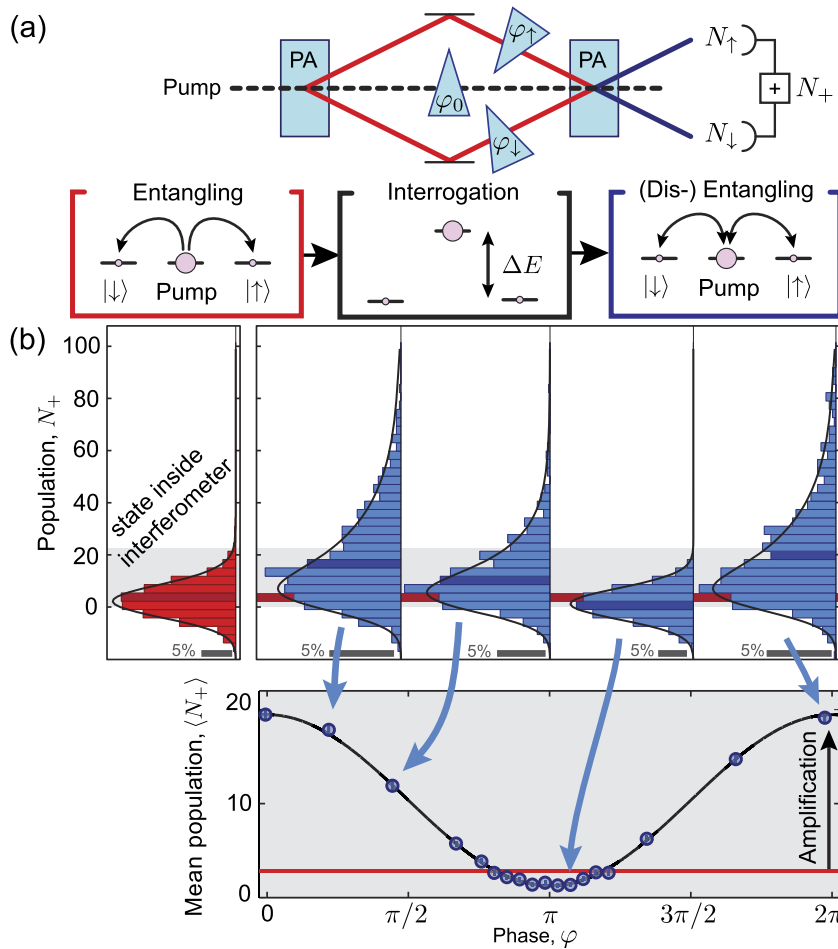


FIG. 12. Atomic SU(1,1) interferometer. (a) Interferometric scheme with the wave splitting and recombination processes equivalent to parametric amplifiers (PAs). (b) The output atomic number distributions as the phase of the atomic waves changes. Reproduced with permission from Linnemann *et al.* Phys. Rev. Lett. **117**, 013001 (2016). Copyright 2016 American Physical Society.

where $\Gamma = \gamma\alpha$ is the effective opto-mechanical coupling rate. The first term in Eq. (41) has the form of the well-known beam splitter Hamiltonian, whereas the second term is similar to a parametric amplification process given in Eq. (10). The derivation above is oversimplified without considering the multi-mode nature of the optical field. With a multi-mode model, the interaction can be viewed as a Raman process so that the second term in Eq. (41) corresponds to the Stokes scattering, while the first term corresponds to the anti-Stokes scattering. Whichever term dominates the interaction depends on the cavity resonance to the Stokes or anti-Stokes component of the optical field. In analogy with a Ramsey interferometer, Qu *et al.*⁹⁰ utilized the beam splitter-like Hamiltonian in the first term of Eq. (41) to realize an opto-mechanical Ramsey interferometer. Of course, had they used the second term of Eq. (41), it would have become a hybrid photon-phonon SU(1,1) interferometer in the same spirit of the atom-light hybrid interferometer discussed in Sec. V B.

For an all-phonon SU(1,1) interferometer, strong nonlinear interaction between mechanical oscillators is required. This was realized by Patil *et al.*,⁹¹ who demonstrated parametric amplification of phonons and thermo-mechanical noise squeezing. Equipped with phonon parametric amplifiers, Cheung *et al.*⁹² realized a PA + BS

version of the all-phonon SU(1,1) interferometer (Sec. IV A) where the second parametric amplifier is replaced by a beam splitter.

VI. APPLICATIONS OF SU(1,1) INTERFEROMETERS

The primary application of SU(1,1) interferometers is in phase measurement. It was shown in Sec. III D that the phase measurement sensitivity can beat the standard quantum limit. On the other hand, as we have found in Sec. III C 1, the noise reduction in SU(1,1) is due to quantum destructive interference, which reduces all noise of the whole output fields of the interferometer. So, the sensitivity enhancement effect is not limited to phase measurement and can also be applied to the measurement of other quadrature-phase amplitudes such as amplitude measurement, as we will show next.

A. Multi-parameter measurement

As is well known, phase and amplitude are conjugate variables so that the Heisenberg uncertainty principle prevents their simultaneous measurement with precision beyond what the uncertainty principle allows. However, this limitation is on one object and the entanglement between two objects can break this limitation, which is what leads to the famous EPR paradox in an

apparent violation of the Heisenberg uncertainty relation.^{49,50,93} However, Braunstein and Kimble⁵⁷ made use of this seemingly contradicting behavior of the entangled source to achieve simultaneous measurement of phase and amplitude with measurement precision, beating the limit set by the Heisenberg uncertainty relation. The experimental demonstration of this phenomenon was first performed by Li *et al.*⁹⁴ following a proposal by Zhang and Peng,⁹⁵ which is a variation of the quantum dense coding scheme of Braunstein and Kimble.⁵⁷ More recently, Steinlechner *et al.*⁹⁶ applied the same technique to a prototype interferometer for gravitational wave detection with simultaneous measurement of two non-orthogonal quantities.

A look at the quantum dense coding scheme by Braunstein and Kimble reveals that it is just the PA + BS scheme of the SU(1,1) interferometer that we discussed in Sec. IV A. Since the role of the BS is the same as the second parametric amplifier in the SU(1,1) interferometer to superpose the two entangled fields, the original SU(1,1) interferometer with two parametric amplifiers should be able to accomplish the same task as the quantum dense coding scheme. Indeed, it was theoretically shown⁶¹ that while homodyne detection of \hat{Y}_1 at the signal output port of PA2 (port 1 in Fig. 3) gives rise to the measurement of the phase modulation δ with an SNR of

$$SNR_{Ph}^{(1)} = \frac{4g_2^2 I_{ps} \delta^2}{(G_1^2 + g_1^2)(G_2^2 + g_2^2) - 4G_1 G_2 g_1 g_2} \rightarrow 2(G_1 + g_1)^2 I_{ps} \delta^2 \text{ for } g_2 > g_1 \text{ and } g_1 \gg 1, \quad (42)$$

as presented in Eq. (21), homodyne detection of \hat{X}_2 at the idler output port of PA2 (port 2 in Fig. 3) leads to the measurement of the amplitude modulation with an SNR of

$$SNR_{Am}^{(2)} = \frac{4G_2^2 I_{ps} \epsilon^2}{(G_1^2 + g_1^2)(G_2^2 + g_2^2) - 4G_1 G_2 g_1 g_2} \rightarrow 2(G_1 + g_1)^2 I_{ps} \epsilon^2 \text{ for } g_2 > g_1 \text{ and } g_1 \gg 1, \quad (43)$$

where ϵ is the amplitude modulation signal. Similar to the phase measurement sensitivity given in Eq. (42), the sensitivity of the amplitude measurement presented in Eq. (43) also beats the standard quantum limit. Figure 13 shows the schematic of the SU(1,1) interferometer for the simultaneous measurement of both a phase shift δ and an amplitude change ϵ in the signal field. Note that the phase measurement [HD1 for $\hat{X}_s(\phi_1)$ with $\phi_1 = \pi/2$] and amplitude measurement [HD2 for $\hat{X}_i(\phi_2)$ with $\phi_2 = 0$] are performed at different ports (signal and idler output ports) that are independent of each other. Therefore, we can make the simultaneous measurement of encoded phase and amplitude signals with their sensitivities simultaneously beating the standard quantum limit.

The above application of the SU(1,1) interferometer to the simultaneous measurement of phase and amplitude was experimentally demonstrated by Liu *et al.*¹⁹ Furthermore, the measurement scheme is extended to simultaneous measurement of multiple non-commuting observables, which are not necessarily orthogonal [HD1 for $\hat{X}_s(\phi_1)$, HD2 for $\hat{X}_s(\phi_2)$, HD3 for $\hat{X}_{s'}(\phi_3)$ in Fig. 13 with arbitrary ϕ_1, ϕ_2, ϕ_3]. Since outputs are amplified, we can further split the signal output without introducing vacuum noise for the simultaneous measurement of another modulation non-orthogonal to phase and amplitude by HD3 of $\hat{X}_{s'}(\phi_3)$.

The advantages of the SU(1,1) interferometer over the quantum dense coding scheme⁵⁷ are as follows: (1) more than two non-commuting quantities can be simultaneously measured and (2) it is tolerant to propagation and detection losses.

B. Quantum resource sharing

When using SU(1,1) interferometers for the simultaneous measurement of phase and amplitude, there exists an interesting relation between the optimum sensitivities of the two measurements. Expressed in terms of the signal-to-noise ratios, the relation is written as^{61,97}

$$SNR_{Ph} + SNR_{Am} = SNR_{op}, \quad (44)$$

where SNR_{op} is the optimized SNR of the corresponding measurement when the resource is all devoted to that measurement so that it is impossible to make the other measurement. This can be seen from Eqs. (42) and (43) where, if we set the modulation signals equal, $\delta = \epsilon$, and add the two SNRs, we have

$$SNR_{Ph}^{(1)} + SNR_{Am}^{(2)} = 4(G_1 + g_1)^2 I_{ps} \delta^2 = SNR_{op}, \quad (45)$$

where SNR_{op} is given by Eq. (33) for the optimum phase measurement sensitivity obtained in the dual-beam scheme. In fact, the less-than-optimized results in Eq. (32) for finite g_1 in the dual beam scheme can be attributed to the relation in Eq. (45) of quantum resource sharing. When Y_1 is measured for the phase modulation signal, the other port can still be used for amplitude measurement, but a straightforward calculation gives an SNR of

$$SNR_{Am}^{(2)} = 2I_{ps} \epsilon^2 / (G_1^2 + g_1^2), \quad (46)$$

where we set $g_2 > g_1$ and $G_2 \approx g_2 \gg 1$ for the optimum value and ϵ is the amplitude modulation signal. This, when set to have $\epsilon = \delta$, together with the SNR for phase modulation in Eq. (32) leads to Eq. (45) for quantum resource sharing even at finite g_1 . Furthermore, although the phase measurement result of the joint measurement between the two ports in Eq. (33) gives SNR_{op} , since both ports are used for phase measurement, which leaves no room for amplitude measurement, namely, $SNR_{Am} = 0$, this again satisfies Eq. (45) for

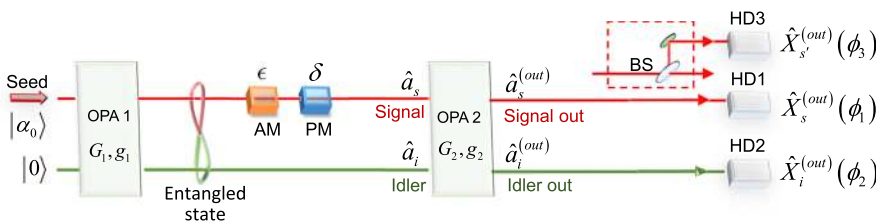


FIG. 13. Simultaneous phase (δ) and amplitude (ϵ) measurement by using an SU(1,1) interferometer. HD: homodyne detection and BS: beam splitter. Reproduced with permission from Liu *et al.* Opt. Express **26**, 27705 (2018). Copyright 2018 Optical Society of America.

quantum resource sharing. Note from Eq. (46) that when $g_1 \rightarrow \infty$, $SNR_{Am}^{(2)} \rightarrow 0$, indicating that the dual-beam scheme discussed in Sec. IV C is not suitable for amplitude modulation measurement. The reason for this can be traced to the intensity correlation between the two entangled fields from the first parametric amplifier or the so-called twin beam effect:⁹⁸ noise in the intensity difference is reduced due to intensity correlation, whereas the amplitude modulation signal encoded in the two fields is also canceled, leading to no amplitude modulation signal in the intensity difference.

C. Quantum information tapping

It is well known⁹⁹ that when quantum information is split with a beam splitter, vacuum noise comes in from the unused port, leading to degradation of SNRs of the split signals as compared to the input. Shapiro suggested using squeezed states to combat the vacuum noise and preserve the SNRs of the split signals.⁹⁹ This is the so-called quantum information tapping. Such a scheme was implemented by Bruckmeier *et al.*¹⁰⁰

The SU(1,1) interferometer discussed here can be used for quantum information tapping. Consider the two outputs of PA2. We have from Eq. (23) for $g_2 > g_1$ and $G_2 \approx g_2 \gg 1$

$$SNR_{SU(1,1)}^{(1)} = SNR_{SU(1,1)}^{(2)} = 2(G_1 + g_1)^2 I_{ps} \delta^2. \quad (47)$$

So, the two outputs are identical copies of each other, which can be thought of as the two split signals for the modulated phase signal encoded to the input field before PA2. The input SNR is obtained from the direct measurement and is given as $SNR_{in} = 2(G_1 + g_1)^2 \delta^2 I_{ps}$.⁶¹ Hence, we have the transfer coefficients, which are defined as $\mathcal{T}^{(1,2)} \equiv SNR_{SU(1,1)}^{(1,2)} / SNR_{in}$, satisfying the relation for quantum information tapping,

$$\mathcal{T}^{(1)} + \mathcal{T}^{(2)} = 2. \quad (48)$$

Note that the classical tapping limit is $\mathcal{T}^{(1)} + \mathcal{T}^{(2)} \leq 1$.⁹⁹ The experimental implementation of the quantum information tapping scheme from an SU(1,1) interferometer was realized by Guo *et al.*,¹⁷ which is basically the amplifier version¹⁰¹ of quantum information tapping but with quantum entangled fields as the input in order to achieve noiseless quantum amplification.^{59,60} A variation of this scheme is the much improved dual-beam encoding scheme in an SU(1,1) interferometer.⁶⁹ It was demonstrated for the first time by the quantum information tapping technique that a quantum enhanced signal can be split into two while still maintaining the quantum enhancement property. The SU(1,1) scheme of quantum information tapping was extended by Liu *et al.*¹⁰² to a three-way quantum information tapping scheme for quantum information cascading.

D. Measurement of entanglement in continuous variables

Verification of quantum entanglement between two light sources is a basic experimental technique in quantum information. For continuous variables, it is usually done via the homodyne detection technique by directly measuring the quadrature-phase amplitude correlations of the two fields: $\langle \Delta^2 \hat{X}_- \rangle$ and $\langle \Delta^2 \hat{Y}_+ \rangle$ with $\hat{X}_- \equiv \hat{X}_1 - \hat{X}_2$ and $\hat{Y}_+ \equiv \hat{Y}_1 + \hat{Y}_2$.^{49,50,103,104} Quantum entanglement

satisfies the inseparability criterion: $I \equiv \frac{1}{4}(\langle \Delta^2 \hat{X}_- \rangle + \langle \Delta^2 \hat{Y}_+ \rangle) < 1$.¹⁰⁵ However, this traditional homodyne method is prone to loss, which severely limits the application of entanglement. On the other hand, as we have shown in Sec. III A, parametric amplifiers (PAs) can act as non-conventional beam splitters for mixing of two fields, which is exactly performed when quantities $\hat{X}_- \equiv \hat{X}_1 - \hat{X}_2$ and $\hat{Y}_+ \equiv \hat{Y}_1 + \hat{Y}_2$ are measured, forming an SU(1,1)-type interferometer. We analyze this scheme next.

As shown in Fig. 14, the two fields \hat{a}_1 and \hat{a}_2 , whose entanglement property needs to be characterized, enter the input ports of a parametric amplifier (PA) of amplitude gain parameters G, g . We perform homodyne detections (HD1, HD2) at the two outputs, one for the X-quadrature ($\hat{X}_1^{(o)}$) and the other for the Y-quadrature ($\hat{Y}_2^{(o)}$), similar to the scheme of joint measurement of phase and amplitude. According to Eq. (12), we obtain the input and output relations for the X, Y-quadratures as

$$\hat{X}_{1,2}^{(o)} = G\hat{X}_{1,2} - g\hat{X}_{2,1}, \quad \hat{Y}_{1,2}^{(o)} = G\hat{Y}_{1,2} + g\hat{Y}_{2,1}, \quad (49)$$

where we dropped the input label (*in*) for clarity and added a π phase to g so that it changes sign. Then, the results of measurement are

$$\begin{aligned} \langle \Delta^2 \hat{X}_1^{(o)} \rangle &= \langle \Delta^2 (G\hat{X}_1 - g\hat{X}_2) \rangle \\ &= G^2 \langle \Delta^2 (\hat{X}_1 - k\hat{X}_2) \rangle = G^2 \langle \Delta^2 \hat{X}_-^{(k)} \rangle, \\ \langle \Delta^2 \hat{Y}_1^{(o)} \rangle &= \langle \Delta^2 (G\hat{Y}_1 + g\hat{Y}_2) \rangle \\ &= G^2 \langle \Delta^2 (\hat{Y}_1 + k\hat{Y}_2) \rangle = G^2 \langle \Delta^2 \hat{Y}_+^{(k)} \rangle, \end{aligned} \quad (50)$$

where $k \equiv g/G \rightarrow 1$ for large G and $\hat{X}_-^{(k)} \equiv \hat{X}_1 - k\hat{X}_2$, $\hat{Y}_+^{(k)} \equiv \hat{Y}_1 + k\hat{Y}_2$. If we block the two inputs and make measurement for vacuum input, we can obtain the result of uncorrelated vacuum for comparison. Taking the ratio for the two measurements, we have

$$\begin{aligned} I_{amp}^{(1,2)} &\equiv \frac{\langle \Delta^2 \hat{X}_{1,2}^{(o)} \rangle + \langle \Delta^2 \hat{Y}_{1,2}^{(o)} \rangle}{\langle \Delta^2 \hat{X}_{1,2}^{(o)} \rangle_v + \langle \Delta^2 \hat{Y}_{1,2}^{(o)} \rangle_v} \\ &= \frac{\langle \Delta^2 \hat{X}_-^{(k)} \rangle + \langle \Delta^2 \hat{Y}_+^{(k)} \rangle}{2(1+k^2)} \rightarrow I \text{ for } k \rightarrow 1. \end{aligned} \quad (51)$$

Therefore, we can make direct measurement of the inseparability quantity I with a high gain parametric amplifier ($k \rightarrow 1$). The advantage is its tolerance to any loss at detection (L_D), as in all applications

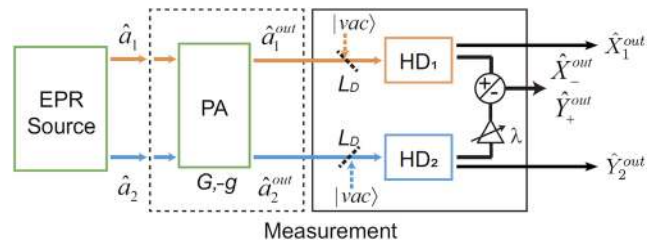


FIG. 14. Entanglement measurement with the help of a parametric amplifier (PA). HD: homodyne detection. L_D : detection loss. Reproduced with permission from Li *et al.*, Phys. Rev. A **101**, 053801 (2020). Copyright 2020 American Physical Society.

of SU(1,1) interferometers. The other advantage is the simultaneous measurement of \hat{X}_-, \hat{Y}_+ with no parameter adjustment. The disadvantage is the need to have a relatively high gain.

Furthermore, if we make joint measurement for the quantities $\hat{X}_-^{(o)} \equiv \hat{X}_1^{(o)} - \lambda \hat{X}_2^{(o)}$ and $\hat{Y}_+^{(o)} \equiv \hat{Y}_1^{(o)} + \lambda \hat{Y}_2^{(o)}$ at the two outputs, one at a time, it can be shown¹⁰⁶ that with a proper adjustment of the electronic coefficient $\lambda = (kG - g)/(G - kg)$, we can always obtain

$$I_{amp}^{JM} = \frac{\langle \Delta^2 \hat{X}_-^{(o)} \rangle + \langle \Delta^2 \hat{Y}_+^{(o)} \rangle}{\langle \Delta^2 \hat{X}_-^{(o)} \rangle_\nu + \langle \Delta^2 \hat{Y}_+^{(o)} \rangle_\nu} = \frac{\langle \Delta^2 \hat{X}_-^{(k)} \rangle + \langle \Delta^2 \hat{Y}_+^{(k)} \rangle}{2(1 + k^2)} = I^{(k)} \quad (52)$$

for any gain parameters G, g . Notably, we have $I_{amp}^{JM} = I$ with $\lambda = 1$. Note that when $G = 1, g = 0$, this is exactly the method of direct homodyne measurement,^{49,50,103,104} but with the help of a parametric amplifier of $G, g \gg 1$, the scheme is immune to losses.

The discussion above is for the single-mode case. For the multi-mode case, parametric amplifiers have the ability to select the dominating mode.¹⁰⁶ This is because different modes have different parametric gains. In the high gain limit, the mode with the largest gain will dominate. Thus, application of parametric amplifiers to entanglement measurement can also filter out unwanted higher order modes and concentrate on the dominating mode. By using the mode engineering technique on parametric amplifiers discussed in Sec. VI E, we can select the mode of our interest.

The scheme discussed above for entanglement measurement was implemented experimentally by Li *et al.*⁶⁴ with fiber optical parametric amplifiers, demonstrating the loss-tolerant and mode selecting properties for the high gain case.

E. Mode engineering of quantum states with SU(1,1) interferometers

Another interesting application of SU(1,1) interferometers is the modification of the mode structure of the quantum state in the output fields to achieve quantum state engineering. The mode structure of quantum states has recently attracted a lot of attention because it increases the degrees of freedom for quantum fields and is especially appealing to quantum information science because of its ability to achieve multi-dimensional quantum entanglement (see a comprehensive review by Fabre and Treps¹⁰⁷). Modes of photons play essential roles in quantum interference because they define the identity of photons and often lead to distinguishability.¹⁰⁸ It is crucial to have mode match between interfering fields in order to achieve high visibility. Our discussion so far on SU(1,1) interferometers has assumed perfect mode match. Multi-mode behavior of SU(1,1) is also quite different from linear interferometers. In fact, a recent work demonstrated the mode cleaning ability of SU(1,1).^{64,106} In the following, we will discuss the ability of SU(1,1) for tailoring the mode structure of quantum fields to our need.

The modification of the mode structure is achieved by engineering the phase change in between the two PAs. This idea was put into action^{31,32} soon after the first experimental realization of the SU(1,1) interferometers.^{12,13} It can be used to modify both spatial^{31,109,110} and temporal/spectral^{32,111–115} profiles of the output fields. More recently, a multi-stage SU(1,1) (Sec. IV D) was implemented for precise and versatile engineering of the spectral mode function of the output quantum states.¹¹⁶ As an example, we present

here the interferometric scheme to achieve flexible and precise spectral mode engineering for the two-photon state produced from spontaneous parametric emission (SPE) processes.

When pumped by an ultra-short pulse (~ 100 fs), SPE processes generate a broadband two-photon state of the form similar to Eq. (35) but with a multi-frequency mode description,

$$|\Psi_2\rangle = |vac\rangle + g \int d\Omega_s d\Omega_i F(\Omega_s, \Omega_i) \hat{a}_s^\dagger(\Omega_s) \hat{a}_i^\dagger(\Omega_i) |vac\rangle, \quad (53)$$

where $F(\Omega_s, \Omega_i)$ is the normalized joint spectral function (JSF) describing the joint spectral properties of the signal (subscript s) and idler (subscript i) photons and has the form of

$$F(\Omega_s, \Omega_i) = \mathcal{N} e^{-(\Omega_s + \Omega_i)^2 / 2\sigma_p^2} \text{sinc}(\Delta k L / 2), \quad (54)$$

with Δk as the wave vector (phase) mismatch among all the waves in a nonlinear medium of length L . $g (\ll 1)$ is similar to the same quantity in Eq. (35). It is proportional to L and the nonlinear coefficient and is related to the peak amplitude of the pump field. \mathcal{N} is the normalization constant. Note that Eq. (54) is written in terms of the frequency offsets Ω_s, Ω_i ($\Omega_l \equiv \omega_l - \omega_{l0}, l = s, i$) from the central frequencies ω_{s0}, ω_{i0} of the generated fields, which are determined by the phase matching condition $\Delta k = 0$ and the center frequency of the pump field.

If the frequencies of the signal and idler photons are close to each other, that is, $|\omega_{s0} - \omega_{i0}| \ll \omega_{s0}, \omega_{i0}$, then the sinc-function in $F(\Omega_s, \Omega_i)$ has a broad bandwidth much wider than the pump bandwidth σ_p . In this case, $F(\Omega_s, \Omega_i)$ is mainly determined by the exponential function and forms a strip along -45° , as shown in Fig. 15(a). The strip orientation of -45° reflects the frequency anti-correlation between the signal and idler photons due to energy conservation of photons. This shape of JSF gives rise to a two-photon state with multiple temporal modes and is not desirable for quantum interference in quantum information applications. Single-mode two-photon states are preferable, corresponding to a factorable JSF with a shape such as a round circle.

The JSF of the two-photon state can be modified by using an SU(1,1) interferometer with a spectrally dependent phase θ by using

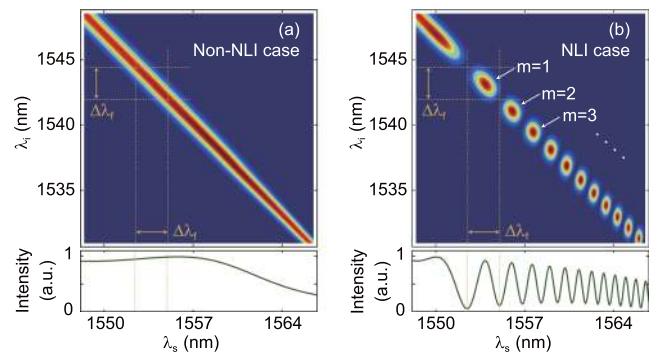


FIG. 15. Contour plot of the joint spectral function $F(\Omega_s, \Omega_i)$ (JSF) of a two-photon state generated from four-wave mixing processes in optical fibers, but the variables are in wavelengths, as in the original paper¹¹³ ($\Omega_l \equiv \omega_l - \omega_{l0}, \lambda_l = 2\pi c/\omega_l, l = s, i$). (a) A single parametric process. (b) An SU(1,1) interferometer with spectrally dependent phase for the modification of JSF. Marginal intensity distribution $I(\Omega_s)$ is below the horizontal axes. Reproduced with permission from Su *et al.*, Opt. Express **27**, 20479 (2019). Copyright 2019 Optical Society of America.

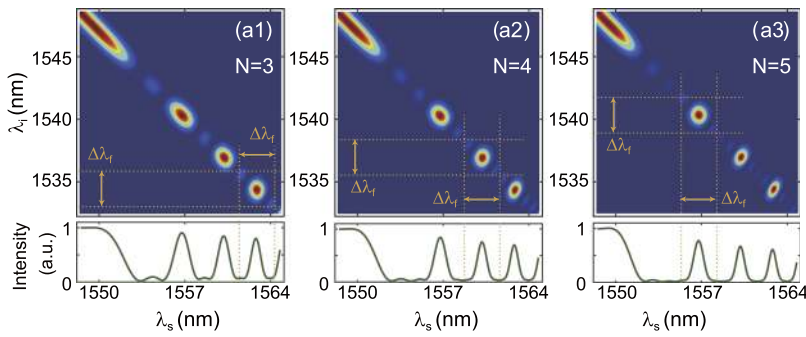


FIG. 16. Contour plot of the joint spectral function $F(\Omega_s, \Omega_i)$ (JSF) for the output state from a multi-stage SU(1,1) interferometer. $N =$ (a1) 3, (a2) 4, and (a3) 5. The variables are in wavelengths as in Fig. 15. Reproduced with permission from Su *et al.*, Opt. Express **27**, 20479 (2019). Copyright 2019 Optical Society of America.

a linear dispersive medium sandwiched in between the two PAs, as shown in Fig. 9 with $N = 2$. Then, the interference term $H(\theta) = 2 \cos \theta$ in Eq. (37) will modify the single PA term g or the JSF $F(\Omega_s, \Omega_i)$ in Eq. (54) for the broadband case. For the case of near degenerate frequencies of $|\omega_{s0} - \omega_{i0}| \ll \omega_{s0}, \omega_{i0}$, the first-order dispersion disappears and second-order dispersion leads to $\theta = \beta(\Omega_s - \Omega_i)^2 L_{DM}$ with β being proportional to the second-order dispersion coefficient and L_{DM} as the length of the linear dispersive medium. Figure 15(b) shows the modified JSF together with the marginal intensity $I(\omega_s)$ of the signal field, showing the interference fringe. The island structure of the modified JSF is a result of two-photon interference and forms a multi-dimensional two-photon state with entanglement between different islands.¹¹⁷ Filters can be used to select the roundest island for a nearly factorable JSF (yellow dashed lines). The shape of the islands can be adjusted depending on the pump bandwidth σ_p and the length L_{DM} of the dispersive medium.

The cleanliness and thus better quality of the selected island depend on the visibility of interference. This can be improved with a multi-stage design, presented in Sec. IV D, where the interference term $H(\theta) = \frac{\sin N\theta/2}{\sin \theta/2}$ will make the islands well separated with increasing stage number N , as shown in Fig. 16. The improved visibilities in the interference pattern shown in the marginal intensity should give a cleaner JSF with better quality as N increases. However, the well-known mini-peaks of the $H(\theta)$ function between the main islands are troublesome. Further shaping of the $H(\theta)$ function can be done with a design of uneven gain g_k or gain medium length $L_k (g_k \propto L_k)$ distribution among N PAs. It was shown that a binomial distribution $L_k = L_1(N-1)!/(k-1)!(N-k)!$ ($k = 1, 2, \dots, N$) will eliminate the mini-peaks, leading to an improved JSF.¹¹⁸

With SU(1,1) interferometers, there are many degrees of freedom for adjustment and fine tuning in the modification of the JSF of the two-photon state to achieve what we want. Although the discussion is for the low gain case ($g \ll 1$), it was shown experimentally that the interferometric technique works equally well in the high gain regime for the precise engineering of the mode structure of entangled fields in continuous variables.^{111,112,115,118} However, all the theoretical treatment^{112,118} in this case does not consider the non-commuting property of the Hamiltonian between different PAs.⁷¹

VII. SUMMARY AND FUTURE PROSPECTS

SU(1,1) interferometers are a new type of interferometers that employ nonlinear interactions such as parametric processes to split

and mix beams for interference. They possess some unique properties, making them advantageous over the traditional beam splitter-based interferometers. These properties include higher sensitivity, detection loss tolerance, and mixing of different types of waves. A key feature of the interferometer is the quantum correlation between the two interfering arms of the interferometer, which is responsible for the enhancement of phase measurement sensitivity. The involvement of the parametric amplifier in the superposition of the interfering waves leads to the loss tolerance property that has some practical implications in quantum metrology. The nonlinear mixing of different types of waves for interference opens up doors for potentially much wider application of this new type of interferometer than the traditional interferometers. These advantages originate from the employment of parametric amplifiers in the interferometers. Parametric amplifiers are active elements requiring strong pumping and are thus very resource intensive. Despite these demonstrated advantages, we still have many challenges, both fundamental and technological, in the further development of the technique of SU(1,1) interferometers.

Among these advantageous properties, the ability to mix waves of different types in SU(1,1) interferometers will make them more promising than others for sensing applications in wide areas. It will be especially attractive to those waves that lack an efficient way of detection such as THz and far infrared waves. SU(1,1) interferometers allow sensing of phase changes in these waves but make detection at other waves for which detection efficiency is high, so long as there is a coupling between these waves for nonlinear mixing. In fact, this idea has already been applied to spectral sensing and imaging of an object with photons at one wavelength but detecting at another.^{28,37–41} This should also widen our capability to construct sensors for measuring a variety of physical quantities through these waves. For example, coupling an atomic de Broglie wave through translational degrees of freedom to light by super-radiance^{87,88,119} will allow us to sense gravitational field. An all-matter wave SU(1,1) interferometer can also be used to measure gravity and will require matter wave mixing⁸⁵ for its realization. To make these applications possible, we need to look for nonlinear mixing between waves of our interest. Of course, these interactions may not be in the form of parametric interaction given in Eq. (10) and the interferometers constructed with them will not be SU(1,1)-type as we discussed in this paper. They will have totally different properties yet to be explored. An example is the engineered multi-particle interaction for phonons in trapped ion systems.¹²⁰

The experimental realizations discussed in this paper are mostly proof-of-principle experiments, and they are operated under relatively small phase sensing photon numbers (I_{ps}). For their wide applications in sensing, we still need to see how they can be adapted to practical situations and different environments. For example, for surpassing the performance of traditional interferometers in actual sensing applications, we need to increase the absolute sensitivity. This is achieved by increasing the phase sensing photon number I_{ps} . However, this usually leads to saturation of the parametric amplifiers and other unwanted nonlinear effects such as self-phase modulation in optical fibers. Perhaps, the solution to this problem lies in the selection of operating points at relatively low overall gain of the interferometer with double injection, as suggested in Ref. 10 and realized in Ref. 94. A recent proposal suggests to tap some of the pump photons for sensing to increase I_{ps} .²⁵ Different applications require different variations of SU(1,1) interferometers. For example, how can SU(1,1) interferometers be adapted to measure rotation like Sagnac interferometers do? This is not obvious since the SU(1,1) interferometers depend on the phase sum instead of phase difference.

To take the quantum advantages for realization of quantum sensing, we need to have an effective way to control the internal losses of the interferometers. Although SU(1,1) interferometers are relatively immune to external losses such as detection inefficiency, what limits the enhancement of sensitivity is the internal losses experienced by the fields in between the two PAs or the losses suffered by the PAs.^{11,66} These losses will introduce uncorrelated vacuum noise that cannot be canceled by quantum destructive interference, leading to extra noise and reducing SNRs. This is not fundamental but poses practical challenges in device construction.

As we discussed at the end of Secs. IV D and VI E, the high gain case in multi-stage SU(1,1) has not been treated theoretically because of the issue of non-commuting Hamiltonian of different PAs. The high gain regime of the parametric amplifier is important because it can generate EPR-type quantum entanglement in continuous variables.^{49,50} It is the basis for complete quantum state teleportation and quantum metrology applications. Thus, this will be a challenge for future theoretical investigation of SU(1,1).

SU(1,1) interferometers have the potential to reach the ultimate Heisenberg limit (HL) of phase measurement sensitivity. However, as we have seen, internal losses are the main obstacle for improving sensitivity. How will losses affect the ability of SU(1,1) interferometers to reach the Heisenberg limit?

The approach of SU(1,1) interferometers is to change the structures of interferometers by replacing beam splitters with parametric amplifiers. This is in contrast to the approach of inputting different quantum states for sensing in traditional interferometers. It is known that parametric amplifiers are quantum devices producing quantum states by themselves, whereas beam splitters are classical devices that do not produce quantum states by themselves but rely on the injection of quantum states to achieve quantum sensing. The former approach can be thought of as the hardware change of devices, whereas the latter as the software programming of input states. The general condition for optimum quantum states was derived before.⁸ Is there an optimum interaction or hardware design in the construction of the non-traditional interferometers for sensing or other applications? Answer to this and other

forementioned questions will likely broaden our knowledge and applications of non-traditional interferometers.

ACKNOWLEDGMENTS

The authors would like to thank the support from the National Natural Science Foundation of China (Grant Nos. 11527808 and 91736105), the National Key Research and Development Program of China (Grant No. 2016YFA0301403), and the US National Science Foundation (Grant No. 1806425).

DATA AVAILABILITY

Data sharing is not applicable to this article as no new data were created or analyzed in this study.

REFERENCES

- C. M. Caves, "Quantum-mechanical noise in an interferometer," *Phys. Rev. D* **23**, 1693 (1981).
- M. Xiao, L.-A. Wu, and H. J. Kimble, "Precision measurement beyond the shot-noise limit," *Phys. Rev. Lett.* **59**, 278 (1987).
- P. Grangier, R. E. Slusher, B. Yurke, and A. LaPorta, "Squeezed-light-enhanced polarization interferometer," *Phys. Rev. Lett.* **59**, 2153 (1987).
- J. Abadie *et al.*, "A gravitational wave observatory operating beyond the quantum shot-noise limit," *Nat. Phys.* **7**, 962 (2011).
- H. Grote, K. Danzmann, K. L. Dooley, R. Schnabel, J. Slutsky, and H. Vahlbruch, "First long-term application of squeezed states of light in a gravitational-wave observatory," *Phys. Rev. Lett.* **110**, 181101 (2013).
- R. Schnabel, "Squeezed states of light and their applications in laser interferometers," *Phys. Rep.* **684**, 1 (2017).
- B. Yurke, S. L. McCall, and J. R. Klauder, "SU(2) and SU(1,1) interferometers," *Phys. Rev. A* **33**, 4033 (1986).
- Z. Y. Ou, "Fundamental quantum limit in precision phase measurement," *Phys. Rev. A* **55**, 2598 (1997).
- P. M. Anisimov, G. M. Raterman, A. Chiruvelli, W. N. Plick, S. D. Huver, H. Lee, and J. P. Dowling, "Quantum metrology with two-mode squeezed vacuum: Parity detection beats the Heisenberg limit," *Phys. Rev. Lett.* **104**, 103602 (2010).
- W. N. Plick, J. P. Dowling, and G. S. Agarwal, "Coherent-light-boosted, sub-shot noise, quantum interferometry," *New J. Phys.* **12**, 083014 (2010).
- Z. Y. Ou, "Enhancement of the phase-measurement sensitivity beyond the standard quantum limit by a nonlinear interferometer," *Phys. Rev. A* **85**, 023815 (2012).
- J. Jing, C. Liu, Z. Zhou, Z. Y. Ou, and W. Zhang, "Realization of a nonlinear interferometer with parametric amplifiers," *Appl. Phys. Lett.* **99**, 011110 (2011).
- F. Hudelist, J. Kong, C. Liu, J. Jing, Z. Y. Ou, and W. Zhang, "Quantum metrology with parametric amplifier-based photon correlation interferometers," *Nat. Commun.* **5**, 3049 (2014).
- J. M. Lukens, N. A. Peters, and R. C. Pooser, "Naturally stable Sagnac-Michelson nonlinear interferometer," *Opt. Lett.* **41**, 5438 (2016).
- B. E. Anderson, P. Gupta, B. L. Schmittberger, T. Horrom, C. Hermann-Avigliano, K. M. Jones, and P. D. Lett, "Phase sensing beyond the standard quantum limit with a variation on the SU(1,1) interferometer," *Optica* **4**, 752 (2017).
- M. Manceau, G. Leuchs, F. Khalili, and M. Chekhova, "Detection loss tolerant supersensitive phase measurement with an SU(1,1) interferometer," *Phys. Rev. Lett.* **119**, 223604 (2017).
- X. Guo, N. Liu, X. Li, Y. Liu, and Z. Y. Ou, "Noise figure improvement and quantum information tapping in a fiber optical parametric amplifier with correlated quantum fields," *Sci. Rep.* **6**, 30214 (2016).
- J. M. Lukens, R. C. Pooser, and N. A. Peters, "A broadband fiber-optic nonlinear interferometer," *Appl. Phys. Lett.* **113**, 091103 (2018).

- ¹⁹Y. Liu, J. Li, L. Cui, N. Huo, S. M. Assad, X. Li, and Z. Y. Ou, "Loss-tolerant quantum dense metrology with SU(1,1) interferometer," *Opt. Express* **26**, 27705 (2018).
- ²⁰D. Li, C.-H. Yuan, Z. Y. Ou, and W. Zhang, "The phase sensitivity of an SU(1,1) interferometer with coherent and squeezed-vacuum light," *New J. Phys.* **16**, 073020 (2014).
- ²¹D. Li, B. T. Gard, Y. Gao, C.-H. Yuan, W. Zhang, L. Hwang, and J. P. Dowling, "Phase sensitivity at the Heisenberg limit in an SU(1,1) interferometer via parity detection," *Phys. Rev. A* **94**, 063840 (2016).
- ²²S. Adhikari, N. Bhusal, C. You, H. Lee, and J. P. Dowling, "Phase estimation in an SU(1,1) interferometer with displaced squeezed states," *OSA Continuum* **1**, 438 (2018).
- ²³B. E. Anderson, B. L. Schmittberger, P. Gupta, K. M. Jones, and P. D. Lett, "Optimal phase measurements with bright- and vacuum-seeded SU(1,1) interferometers," *Phys. Rev. A* **95**, 063843 (2017).
- ²⁴Q.-K. Gong, X.-L. Hu, D. Li, C.-H. Yuan, Z. Y. Ou, and W. Zhang, "Intramode-correlation-enhanced phase sensitivities in an SU(1,1) interferometer," *Phys. Rev. A* **96**, 033809 (2017).
- ²⁵S. S. Zsigeti, R. J. Lewis-Swan, and S. A. Haine, "Pumped-up SU(1,1) interferometry," *Phys. Rev. Lett.* **118**, 150401 (2017).
- ²⁶X.-L. Hu, D. Li, L. Q. Chen, K. Zhang, W. Zhang, and C.-H. Yuan, "Phase estimation for an SU(1,1) interferometer in the presence of phase diffusion and photon losses," *Phys. Rev. A* **98**, 023803 (2018).
- ²⁷P. D. Maker, R. W. Terhune, M. Nisenoff, and C. M. Savage, "Effects of dispersion and focusing on the production of optical harmonics," *Phys. Rev. Lett.* **8**, 21 (1962).
- ²⁸D. A. Kalashnikov, A. V. Paterova, S. P. Kulik, and L. A. Krivitsky, "Infrared spectroscopy with visible light," *Nat. Photonics* **10**, 98 (2015).
- ²⁹S.-K. Choi, M. Vasilyev, and P. Kumar, "Noiseless optical amplification of images," *Phys. Rev. Lett.* **83**, 1938 (1999).
- ³⁰A. Mosset, F. Devaux, and E. Lantz, "Spatially noiseless optical amplification of images," *Phys. Rev. Lett.* **94**, 223603 (2005).
- ³¹A. M. Pérez, T. Sh. Iskhakov, P. Sharapova, S. Lemieux, O. V. Tikhonova, M. V. Chekhova, and G. Leuchs, "Bright squeezed-vacuum source with 1.1 spatial mode," *Opt. Lett.* **39**, 2403 (2014).
- ³²T. Sh. Iskhakov, S. Lemieux, A. Perez, R. W. Boyd, G. Leuchs, and M. V. Chekhova, "Nonlinear interferometer for tailoring the frequency spectrum of bright squeezed vacuum," *J. Mod. Opt.* **63**, 64 (2015).
- ³³L. Mandel, "Quantum effects in one-photon and two-photon interference," *Rev. Mod. Phys.* **71**, S274 (1999).
- ³⁴Z.-Y. J. Ou, *Multi-Photon Quantum Interference* (Springer, New York, 2007).
- ³⁵E. Knill, R. Laflamme, and G. J. Milburn, "A scheme for efficient quantum computation with linear optics," *Nature* **409**, 46 (2001).
- ³⁶X. Y. Zou, L. J. Wang, and L. Mandel, "Induced coherence and indistinguishability in optical interference," *Phys. Rev. Lett.* **67**, 318 (1991).
- ³⁷G. B. Lemos, V. Borish, G. D. Cole, S. Ramelow, R. Lapkiewicz, and A. Zeilinger, "Quantum imaging with undetected photons," *Nature* **512**(7515), 409 (2014).
- ³⁸A. Hochrainer, M. Lahiri, R. Lapkiewicz, G. B. Lemos, and A. Zeilinger, "Quantifying the momentum correlation between two light beams by detecting one," *Proc. Natl. Acad. Sci. U. S. A.* **114**, 1508 (2017).
- ³⁹A. Hochrainer, M. Lahiri, R. Lapkiewicz, G. B. Lemos, and A. Zeilinger, "Interference fringes controlled by noninterfering photons," *Optica* **4**, 341 (2017).
- ⁴⁰A. V. Paterova, S. M. Maniam, H. Yang, G. Greci, and L. A. Krivitsky, "Hyperspectral infrared microscopy with visible light," *arXiv:2002.05956* (2020).
- ⁴¹I. Kiviatkovsky, H. M. Chrzanowski, E. G. Avery, H. Bartolomeaus, and S. Ramelow, "Microscopy with undetected photons in the mid-infrared," *arXiv:2002.05960* (2020).
- ⁴²M. V. Chekhova and Z. Y. Ou, "Nonlinear interferometers in quantum optics," *Adv. Opt. Photonics* **8**, 104 (2016).
- ⁴³P. Gupta, B. L. Schmittberger, B. E. Anderson, K. M. Jones, and P. D. Lett, "Optimized phase sensing in a truncated SU(1,1) interferometer," *Opt. Express* **26**, 391 (2018).
- ⁴⁴H. P. Yuen and V. W. S. Chan, "Noise in homodyne and heterodyne detection," *Opt. Lett.* **8**, 177 (1983).
- ⁴⁵Z. Y. Ou and Q. Su, "Uncertainty in determining the phase for an optical field due to the particle nature of light," *Laser Phys.* **13**, 1175 (2003).
- ⁴⁶D. F. Walls, "Squeezed states of light," *Nature* **306**, 141 (1983).
- ⁴⁷P. Luca and A. Smerzi, "Mach-Zehnder interferometry at the Heisenberg limit with coherent and squeezed-vacuum light," *Phys. Rev. Lett.* **100**, 073601 (2008).
- ⁴⁸M. D. Lang and C. M. Caves, "Optimal quantum-enhanced interferometry using a laser power source," *Phys. Rev. Lett.* **111**, 173601 (2013).
- ⁴⁹M. D. Reid, "Demonstration of the Einstein-Podolsky-Rosen paradox using nondegenerate parametric amplification," *Phys. Rev. A* **40**, 913 (1989).
- ⁵⁰Z. Y. Ou, S. F. Pereira, H. J. Kimble, and K. C. Peng, "Realization of the Einstein-Podolsky-Rosen paradox for continuous variables," *Phys. Rev. Lett.* **68**, 3663 (1992).
- ⁵¹B. Chen, C. Qiu, S. Chen, J. Guo, L. Q. Chen, Z. Y. Ou, and W. Zhang, "Atom-light hybrid interferometer," *Phys. Rev. Lett.* **115**, 043602 (2015).
- ⁵²J. M. Manley and H. E. Rowe, "Some General Properties of Nonlinear Elements - Part I: General Energy Relations," *Proc. Inst. Radio Eng.* **44**, 904 (1956); see also R. W. Boyd, *Nonlinear Optics*, 3rd ed. (Academic Press, San Diego, 2007).
- ⁵³C. M. Caves, "Quantum limits on noise in linear amplifiers," *Phys. Rev. D* **26**, 1817 (1982).
- ⁵⁴G. J. Milburn, M. L. Steyn-Ross, and D. F. Walls, "Linear amplifiers with phase-sensitive noise," *Phys. Rev. A* **35**, 4443 (1987).
- ⁵⁵Z. Y. Ou, S. F. Pereira, and H. J. Kimble, "Quantum noise reduction in optical amplification," *Phys. Rev. Lett.* **70**, 3239 (1993).
- ⁵⁶Z. Y. Ou, S. F. Pereira, and H. J. Kimble, "Realization of the Einstein-Podolsky-Rosen paradox for continuous variables in nondegenerate parametric amplification," *Appl. Phys. B* **55**, 265 (1992).
- ⁵⁷S. L. Braunstein and H. J. Kimble, "Dense coding for continuous variables," *Phys. Rev. A* **61**, 042302 (2000).
- ⁵⁸J. Kong, Z. Y. Ou, and W. Zhang, "Phase-measurement sensitivity beyond the standard quantum limit in an interferometer consisting of a parametric amplifier and a beam splitter," *Phys. Rev. A* **87**, 023825 (2013).
- ⁵⁹Z. Y. Ou, "Quantum amplification with correlated quantum fields," *Phys. Rev. A* **48**, R1761 (1993).
- ⁶⁰J. Kong, F. Hudelist, Z. Y. Ou, and W. Zhang, "Cancellation of internal quantum noise of an amplifier by quantum correlation," *Phys. Rev. Lett.* **111**, 033608 (2013).
- ⁶¹J. Li, Y. Liu, L. Cui, N. Huo, S. M. Assad, X. Li, and Z. Y. Ou, "Joint measurement of multiple noncommuting parameters," *Phys. Rev. A* **97**, 052127 (2018).
- ⁶²M. Manceau, F. Khalili, and M. Chekhova, "Improving the phase super-sensitivity of squeezing-assisted interferometers by squeeze factor unbalancing," *New J. Phys.* **19**, 013014 (2017).
- ⁶³W. Du, J. Jia, J. F. Chen, Z. Y. Ou, and W. Zhang, "Absolute sensitivity of phase measurement in an SU(1,1) type interferometer," *Opt. Lett.* **43**, 1051 (2018).
- ⁶⁴J. Li, Y. Liu, N. Huo, L. Cui, C. Feng, Z. Y. Ou, and X. Li, "Pulsed entanglement measured by parametric amplifier assisted homodyne detection," *Opt. Express* **27**, 30552 (2019).
- ⁶⁵E. Flurin, N. Roch, F. Mallet, M. H. Devoret, and B. Huard, "Generating entangled microwave radiation over two transmission lines," *Phys. Rev. Lett.* **109**, 183901 (2012).
- ⁶⁶A. M. Marino, N. V. Corzo Trejo, and P. D. Lett, "Effect of losses on the performance of an SU(1,1) interferometer," *Phys. Rev. A* **86**, 023844 (2012).
- ⁶⁷A. Furusawa, J. L. Sorensen, S. L. Braunstein, C. A. Fuchs, H. J. Kimble, and E. S. Polzik, "Unconditional quantum teleportation," *Science* **282**, 706 (1998).
- ⁶⁸R. C. Pooser, N. Savino, E. Batson, J. L. Beckey, J. Garcia, and B. J. Lawrie, "Truncated nonlinear interferometry for quantum enhanced atomic force microscopy," *Phys. Rev. Lett.* **124**, 230504 (2020).
- ⁶⁹Y. Liu, N. Huo, J. Li, L. Cui, X. Li, and Z. Y. Ou, "Optimum quantum resource distribution for phase measurement and quantum information tapping in a dual-beam SU(1,1) interferometer," *Opt. Express* **27**, 11292 (2019).

- ⁷⁰Z. Y. Ou and Y. J. Lu, "Cavity enhanced spontaneous parametric down-conversion for the prolongation of correlation time between conjugate photons," *Phys. Rev. Lett.* **83**, 2556 (1999).
- ⁷¹N. Quesada and J. E. Sipe, "Effects of time ordering in quantum nonlinear optics," *Phys. Rev. A* **90**, 063840 (2014).
- ⁷²W. H. Louisell, *Coupled Mode and Parametric Electronics* (Wiley, New York, 1960).
- ⁷³N. Roch, E. Flurin, F. F. Nguyen, P. Morfin, P. Campagne-Ibarcq, M. H. Devoret, and B. Huard, "Widely tunable, nondegenerate three-wave mixing microwave device operating near the quantum limit," *Phys. Rev. Lett.* **108**, 147701 (2012).
- ⁷⁴L.-M. Duan, M. D. Lukin, J. I. Cirac, and P. Zoller, "Long-distance quantum communication with atomic ensembles and linear optics," *Nature* **414**, 413 (2001).
- ⁷⁵K. Hammerer, A. S. Sørensen, and E. S. Polzik, "Quantum interface between light and atomic ensembles," *Rev. Mod. Phys.* **82**, 1041 (2010).
- ⁷⁶C. Qiu, S. Chen, L. Q. Chen, B. Chen, J. Guo, Z. Y. Ou, and W. Zhang, "Atom-light superposition oscillation and Ramsey-like atom-light interferometer," *Optica* **3**, 775 (2016).
- ⁷⁷S. Y. Chen, L. Q. Chen, Z. Y. Ou, and W. Hang, "Quantum non-demolition measurement of photon number with atom-light interferometers," *Opt. Express* **25**, 31827 (2017).
- ⁷⁸S. Haroche, "Controlling photons in a box and exploring the quantum to classical boundary," *Rev. Mod. Phys.* **85**, 1083 (2013).
- ⁷⁹M. Gabbriellini, L. Pezzé, and A. Smerzi, "Spin-mixing interferometry with Bose-Einstein condensates," *Phys. Rev. Lett.* **115**, 163002 (2015).
- ⁸⁰D. Linnemann, H. Strobel, W. Muessel, J. Schulz, R. J. Lewis-Swan, K. V. Kheruntsyan, and M. K. Oberthaler, "Quantum-enhanced sensing based on time reversal of nonlinear dynamics," *Phys. Rev. Lett.* **117**, 013001 (2016).
- ⁸¹L. Pezzé, A. Smerzi, M. K. Oberthaler, R. Schmied, and P. Treutlein, *Rev. Mod. Phys.* **90**, 035005 (2018).
- ⁸²A. D. Cronin, J. Schmiedmayer, and D. E. Pritchard, "Optics and interferometry with atoms and molecules," *Rev. Mod. Phys.* **81**, 1051 (2009).
- ⁸³S. Inouye, T. Pfau, S. Gupta, A. P. Chikkatur, A. Görlitz, D. E. Pritchard, and W. Ketterle, "Phase-coherent amplification of atomic matter waves," *Nature* **402**, 641 (1999).
- ⁸⁴M. Kozuma, Y. Suzuki, Y. Torii, T. Sugiura, T. Kuga, E. W. Hagley, and L. Deng, "Phase-coherent amplification of matter waves," *Science* **286**, 2309 (1999).
- ⁸⁵L. Deng, E. W. Hagley, J. Wen, M. Trippenbach, Y. Band, P. S. Julienne, J. E. Simsarian, K. Helmerson, S. L. Rolston, and W. D. Phillips, "Four-wave mixing with matter waves," *Nature* **398**, 218 (1999).
- ⁸⁶S. Inouye, A. P. Chikkatur, D. M. Stamper-Kurn, J. Stenger, D. E. Pritchard, and W. Ketterle, "Superradiant Rayleigh scattering from a Bose-Einstein condensate," *Science* **285**, 571 (1999).
- ⁸⁷D. Schneble, G. Campbell, E. Streed, M. Boyd, D. Pritchard, and W. Ketterle, "Raman amplification of matter waves," *Phys. Rev. A* **69**, 041601(R) (2004).
- ⁸⁸Y. Yoshikawa, T. Sugiura, Y. Torii, and T. Kuga, "Observation of super-radiant Raman scattering in a Bose-Einstein condensate," *Phys. Rev. A* **69**, 041603(R) (2004).
- ⁸⁹C. K. Law, "Interaction between a moving mirror and radiation pressure—A Hamiltonian formulation," *Phys. Rev. A* **51**, 2537 (1995).
- ⁹⁰K. Qu, C. Dong, H. Wang, and G. S. Agarwal, "Optomechanical Ramsey interferometry," *Phys. Rev. A* **90**, 053809 (2014).
- ⁹¹Y. S. Patil, S. Chakram, L. Chang, and M. Vengalattore, "Thermomechanical two-mode squeezing in an ultrahigh-Q membrane resonator," *Phys. Rev. Lett.* **115**, 017202 (2015).
- ⁹²H. F. H. Cheung, Y. S. Patil, L. Chang, S. Chakram, and M. Vengalattore, "Nonlinear phonon interferometry at the Heisenberg limit," *arXiv:1601.02324* (2016).
- ⁹³M. D. Reid, P. D. Drummond, W. P. Bowen, E. G. Cavalcanti, P. K. Lam, H. A. Bachor, U. L. Andersen, and G. Leuchs, "The Einstein-Podolsky-Rosen paradox: From concepts to applications," *Rev. Mod. Phys.* **81**, 1727 (2009).
- ⁹⁴X. Li, Q. Pan, J. Jing, J. Zhang, C. Xie, and K. Peng, "Quantum dense coding exploiting a bright Einstein-Podolsky-Rosen beam," *Phys. Rev. Lett.* **88**, 047904 (2002).
- ⁹⁵J. Zhang and K. Peng, "Quantum teleportation and dense coding by means of bright amplitude-squeezed light and direct measurement of a Bell state," *Phys. Rev. A* **62**, 064302 (2000).
- ⁹⁶S. Steinlechner, J. Bauchrowitz, M. Meinders, H. Müller-Ebhardt, K. Danzmann, and R. Schnabel, "Quantum dense metrology," *Nat. Photonics* **7**, 626 (2013).
- ⁹⁷S. M. Assad, J. Li, Y. Liu, N. Zhao, Z. Wen, P. K. Lam, Z. Y. Ou, and X. Li, "Accessible precisions for estimating two conjugate parameters using Gaussian probes," *Phys. Rev. Res.* **2**, 023182 (2020).
- ⁹⁸O. Aytür and P. Kumar, "Pulsed twin beams of light," *Phys. Rev. Lett.* **65**, 1551 (1990).
- ⁹⁹J. H. Shapiro, "Optical waveguide tap with infinitesimal insertion loss," *Opt. Lett.* **5**, 351 (1980).
- ¹⁰⁰R. Bruckmeier, H. Hansen, S. Schiller, and J. Mlynek, "Realization of a paradigm for quantum measurements: The squeezed light beam splitter," *Phys. Rev. Lett.* **79**, 43 (1997).
- ¹⁰¹J. A. Levenson, I. Abram, T. Rivera, P. Fayolle, J. C. Garreau, and P. Grangier, "Quantum optical cloning amplifier," *Phys. Rev. Lett.* **70**, 267 (1993).
- ¹⁰²N. Liu, J. Li, X. Li, and Z. Y. Ou, "Three-way noiseless signal splitting in a parametric amplifier with quantum correlation," *Phys. Rev. A* **93**, 063838 (2016).
- ¹⁰³C. Gross, H. Strobel, E. Nicklas, T. Zibold, N. Bar-Gill, G. Kurizki, and M. K. Oberthaler, "Atomic homodyne detection of continuous-variable entangled twin-atom states," *Nature* **480**, 219 (2011).
- ¹⁰⁴J. Peise, I. Kruse, K. Lange, B. Lücke, L. Pezzé, J. Arlt, W. Ertmer, K. Hammerer, L. Santos, A. Smerzi, and C. Klempt, "Satisfying the Einstein-Podolsky-Rosen criterion with massive particles," *Nat. Commun.* **6**, 8984 (2015).
- ¹⁰⁵L.-M. Duan, G. Giedke, J. I. Cirac, and P. Zoller, "Inseparability criterion for continuous variable systems," *Phys. Rev. Lett.* **84**, 2722 (2000).
- ¹⁰⁶J. Li, Y. Liu, N. Huo, L. Cui, X. Li, and Z. Y. Ou, "Measuring continuous-variable quantum entanglement with parametric-amplifier-assisted homodyne detection," *Phys. Rev. A* **101**, 053801 (2020).
- ¹⁰⁷C. Fabre and N. Treps, "Modes and states in quantum optics," *Rev. Mod. Phys.* (to be published), *arXiv:1912.09321*.
- ¹⁰⁸Z. Y. Ou, *Quantum Optics for Experimentalists* (World Scientific, 2017).
- ¹⁰⁹G. Frascella, E. E. Mikhailov, N. Takanashi, R. V. Zakharov, O. V. Tikhonova, and M. V. Chekhova, "Wide-field SU(1,1) interferometer," *Optica* **6**, 1233 (2019).
- ¹¹⁰G. Frascella, R. V. Zakharov, O. V. Tikhonova, and M. V. Chekhova, "Experimental reconstruction of spatial Schmidt modes for a wide-field SU(1,1) interferometer," *Laser Phys.* **29**, 124013 (2019).
- ¹¹¹S. Lemieux, M. Manceau, P. R. Sharapova, O. V. Tikhonova, R. W. Boyd, G. Leuchs, and M. V. Chekhova, "Engineering the frequency spectrum of bright squeezed vacuum via group velocity dispersion in an SU(1,1) interferometer," *Phys. Rev. Lett.* **117**, 183601 (2016).
- ¹¹²P. R. Sharapova, O. V. Tikhonova, S. Lemieux, R. W. Boyd, and M. V. Chekhova, "Bright squeezed vacuum in a nonlinear interferometer: Frequency and temporal Schmidt-mode description," *Phys. Rev. A* **97**, 053827 (2018).
- ¹¹³J. Su, L. Cui, J. Li, Y. Liu, X. Li, and Z. Y. Ou, "Versatile and precise quantum state engineering by using nonlinear interferometers," *Opt. Express* **27**, 20479 (2019).
- ¹¹⁴D. B. Horoshko, M. I. Kolobov, F. Gumpert, I. Shand, F. König, and M. V. Chekhova, "Nonlinear Mach-Zehnder interferometer with ultra broadband squeezed light," *J. Mod. Opt.* **67**, 41 (2020).
- ¹¹⁵N. Huo, Y. Liu, J. Li, L. Cui, X. Chen, R. Palivela, T. Xie, X. Li, and Z. Y. Ou, "Direct temporal mode measurement for the characterization of temporally multiplexed high dimensional quantum entanglement in continuous variables," *Phys. Rev. Lett.* **124**, 213603 (2020).
- ¹¹⁶J. Li, J. Su, L. Cui, T. Xie, Z. Y. Ou, and X. Li, "Generation of pure-state single photons with high heralding efficiency by using a three-stage nonlinear interferometer," *Appl. Phys. Lett.* **116**, 204002 (2020).
- ¹¹⁷C. Reimer, S. Sciara, P. Roztock, M. Islam, L. Romero Cortés, Y. Zhang, B. Fischer, S. Loranger, R. Kashyap, A. Cino, S. T. Chu, B. E. Little, D. J. Moss,

L. Caspani, W. J. Munro, J. Azaña, M. Kues, and R. Morandotti, “High-dimensional one-way quantum processing implemented on d-level cluster states,” *Nat. Phys.* **15**, 148 (2019).

¹¹⁸L. Cui, J. Su, J. Li, Y. Liu, X. Li, and Z. Y. Ou, “Quantum state engineering by nonlinear quantum interference,” *Phys. Rev. A* (to be published), [arXiv:1811.07646v2](https://arxiv.org/abs/1811.07646v2) [quant-ph].

¹¹⁹S. A. Haine, “Information-recycling beam splitters for quantum enhanced atom interferometry,” *Phys. Rev. Lett.* **110**, 053002 (2013).

¹²⁰D. Leibfried, B. DeMarco, V. Meyer, M. Rowe, A. Ben-Kish, J. Britton, W. M. Itano, B. Jelenković, C. Langer, T. Rosenband, and D. J. Wineland, “Trapped-ion quantum simulator: Experimental application to nonlinear interferometers,” *Phys. Rev. Lett.* **89**, 247901 (2002).